

## Thermal neutron capture cross sections of the potassium isotopes

R. B. Firestone,<sup>1</sup> M. Krtička,<sup>2</sup> Zs. Révay,<sup>3,4</sup> L. Szentmiklosi,<sup>3</sup> and T. Belgya<sup>3</sup>

<sup>1</sup>Lawrence Berkeley National Laboratory, Berkeley, California 94720, USA

<sup>2</sup>Charles University in Prague, Faculty of Mathematics and Physics, V Holešovičkách 2, CZ-180 00 Prague 8, Czech Republic

<sup>3</sup>Institute of Isotopes, H-1525 Budapest, Hungary

<sup>4</sup>Forschungsmittelnquelle Heinz Maier-Leibnitz (FRM II), Technische Universität München, Munich, Germany

(Received 5 October 2012; published 13 February 2013)

Precise thermal neutron capture  $\gamma$ -ray cross sections  $\sigma_\gamma$  for  $^{39,40,41}\text{K}$  were measured on a natural potassium target with the guided neutron beam at the Budapest Reactor. The cross sections were internally standardized using a stoichiometric KCl target with well-known  $^{35}\text{Cl}(n,\gamma)$   $\gamma$ -ray cross sections [Révay and Molnár, *Radiochimica Acta* **91**, 361 (2003); Molnár, Révay, and Belgya, *Nucl. Instrum. Meth. Phys. Res. B* **213**, 32 (2004)]. These data were combined with  $\gamma$ -ray intensities from von Egidy *et al.* [von Egidy, Daniel, Hungerford, Schmidt, Lieb, Krusche, Kerr, Barreau, Borner, Brissot *et al.*, *J. Phys. G. Nucl. Phys.* **10**, 221 (1984)] and Krusche *et al.* [Krusche, Lieb, Ziegler, Daniel, von Egidy, Rascher, Barreau, Borner, and Warner, *Nucl. Phys. A* **417**, 231 (1984); Krusche, Winter, Lieb, Hungerford, Schmidt, von Egidy, Scheerer, Kerr, and Borner, *Nucl. Phys. A* **439**, 219 (1985)] to generate nearly complete capture  $\gamma$ -ray level schemes. Total radiative neutron cross sections were deduced from the total  $\gamma$ -ray cross section feeding the ground state,  $\sigma_0 = \Sigma\sigma_\gamma(\text{GS})$  after correction for unobserved statistical  $\gamma$ -ray feeding from levels near the neutron capture energy. The corrections were performed with Monte Carlo simulations of the potassium thermal neutron capture decay schemes using the computer code DICEBOX where the simulated populations of low-lying levels are normalized to the measured cross section depopulating those levels. Comparisons of the simulated and experimental level feeding intensities have led to proposed new spins and parities for selected levels in the potassium isotopes where direct reactions are not a significant contribution. We determined the total radiative neutron cross sections  $\sigma_0(^{39}\text{K}) = 2.28 \pm 0.04$  b,  $\sigma_0(^{40}\text{K}) = 90 \pm 7$  b, and  $\sigma_0(^{41}\text{K}) = 1.62 \pm 0.03$  b from the prompt  $\gamma$ -ray data and the  $\gamma$ -ray transition probability  $P_\gamma(1524.66) = 0.164(4)$  in the  $\beta^-$  decay of  $^{42}\text{K}$  in a low-background counting experiment.

DOI: [10.1103/PhysRevC.87.024605](https://doi.org/10.1103/PhysRevC.87.024605)

PACS number(s): 23.20.Lv, 24.10.Lx, 24.60.Dr, 25.40.Lw

### I. INTRODUCTION

Precise thermal neutron capture  $\gamma$ -ray cross sections  $\sigma_\gamma$  have been measured for all elements with  $Z = 1-83$ , 90, and 92, except for He and Pm, at the Budapest Reactor [1,2]. These data were evaluated together with additional information from the literature to generate the Evaluated Gamma-ray Activation File (EGAF) [3] and were also published in the *Handbook of Prompt Gamma Activation Analysis* [4]. The EGAF  $\sigma_\gamma$  data can be used to determine total radiative thermal neutron capture cross sections  $\sigma_0$  if the level scheme is complete, from  $\sigma_0 = \Sigma\sigma_\gamma(\text{GS}) = \Sigma\sigma_\gamma(\text{CS})$  for transitions feeding the ground state (GS) or deexciting the capture state (CS). Neutron capture level schemes generally only complete for low- $Z$  elements.

For most isotopes a substantial, unresolved  $\gamma$ -ray intensity deexcites the high density of levels near the capture state. This continuum feeding must be accounted for to determine  $\sigma_0$  from the  $\sigma_\gamma$  data. We previously demonstrated for the palladium isotopes [5] that the continuum feeding can be determined with statistical model calculations using the Monte Carlo computer code DICEBOX [6]. DICEBOX generates simulated neutron capture decay schemes based on nuclear level density and photon strength function models. The simulated intensities of transitions populating low-lying levels can be normalized to the experimental cross sections deexciting those levels to determine the unobserved cross section feeding the ground state. Together with the observed cross section feeding the ground state this gives  $\sigma_0$ . The sensitivity of this technique was comparable to that of other methods for the palladium isotopes,

even when only a small number of  $\gamma$  rays were observed. In this paper we apply this technique to the analysis of  $\sigma_0$  in the lighter potassium isotopes where, although direct neutron capture may be important for primary  $\gamma$ -ray transitions, the experimentally observed level schemes are relatively complete.

### II. EXPERIMENT

Neutron capture  $\gamma$ -ray cross sections were measured with the guided neutron beam at the 10-MW Budapest Reactor [1]. Neutrons enter the evacuated target holder and continue to the beam stop at the rear wall of the guide hall. The target station, where both primary and secondary  $\gamma$  rays can be measured in low background conditions, is located 30 m from the reactor. The thermal-equivalent neutron flux was  $2 \times 10^6 \text{ n} \cdot \text{cm}^{-2} \cdot \text{s}^{-1}$  during this experiment.

Prompt  $\gamma$  rays from the target were measured with an  $n$ -type high-purity, 25% efficient, germanium (HPGe) detector with closed-end coaxial geometry located 23.5 cm from the target. The detector is Compton-suppressed by a Bismuth Germanate (BGO)-scintillator guard detector annulus surrounded by 10-cm-thick lead shielding. The counting efficiency was calibrated from 50 keV to 10 MeV with radioactive sources and ( $n,\gamma$ ) reaction gamma rays to a precision of better than 1% from 500 keV to 6 MeV and better than 3% at all other energies [7]. The  $\gamma$ -ray spectra were analyzed using the Hypermet PC program [7,8].

TABLE I. Calibration of the 770.3-keV  $\gamma$ -ray cross section from  $^{39}\text{K}(n, \gamma)$  with  $^{35}\text{Cl}(n, \gamma)$   $\gamma$  rays from an elemental KCl standard.

$E_\gamma$ (Cl) (keV)	Elemental $\sigma_\gamma^a$ (barns)	$\sigma_\gamma(770.3)^b$ (barns)
517.1	$7.80 \pm 0.07$	$1.009 \pm 0.016$
787	$9.09 \pm 0.09^c$	$1.020 \pm 0.016$
1164.9	$9.17 \pm 0.08$	$1.023 \pm 0.016$
1951.1	$\equiv 6.51 \pm 0.02$	$1.012 \pm 0.013$
2863.8	$1.871 \pm 0.017$	$1.011 \pm 0.021$
4979.8	$1.261 \pm 0.013$	$1.025 \pm 0.023$
5715.2	$1.871 \pm 0.021$	$1.024 \pm 0.021$
6110.8	$6.78 \pm 0.08$	$1.024 \pm 0.020$
Adopted value <sup>d</sup>		$1.017 \pm 0.013$

<sup>a</sup>From  $\gamma$ -ray emission probabilities of Molnar *et al.* [10] standardized to the cross section at 1951.1 keV [9].

<sup>b</sup>Isotopic cross section assuming the abundance of  $^{39}\text{K}$  is 93.2581  $\pm$  0.0044% [15].

<sup>c</sup>Cross section for the 786.3 + 788.4 keV doublet.

<sup>d</sup>Weighted average. The uncertainty has been increased to that of the most precise measurement.

Elemental radiative thermal neutron  $\gamma$ -ray cross sections were measured on an 0.02 g stoichiometric, high purity KCl target. Internal calibration of the 770.3-keV  $\gamma$ -ray from  $^{39}\text{K}(n, \gamma)$  was performed using several chlorine  $\gamma$ -ray elemental cross sections, as shown in Table I, assuming the  $\sigma_\gamma(1951.1) = 6.51(2)$  b [9] and using the relative emission probabilities of Molnar *et al.* [10]. For the homogenous target the measured cross section is independent of the neutron flux. No target impurities were observed in the prompt  $\gamma$ -ray calibration spectrum. Both the chlorine and potassium isotopes have a  $1/v$  cross-section energy dependence so the respective  $\gamma$ -ray intensity ratios used in these cross-section calibrations are independent of neutron energy. Although the guided neutron beam energy used in these measurements is subthermal, no correction was necessary for the shape of the neutron energy spectrum, and no fast neutrons were present in the guided neutron beam.

An 0.75 g  $\text{KHCO}_3$  powder, suspended in a teflon bag to reduce the background from the target holder, was irradiated for 43 000 seconds to obtain a higher statistics potassium spectrum without interference from the chlorine  $\gamma$  rays. Weak potassium transition cross sections were calibrated by their relative intensities with respect to the 770.3-keV  $\gamma$  ray. The  $\gamma$  rays were assigned to level schemes for the three potassium isotopes  $^{40}\text{K}$ ,  $^{41}\text{K}$ , and  $^{42}\text{K}$  on the basis of energy and intensity by comparison with data from the Evaluated Nuclear Structure Data File (ENSDF) [11] and with the potassium neutron capture data of von Egidy *et al.* [12] and Krusche *et al.* [13,14]. Isotopic  $\gamma$ -ray cross sections were determined assuming the normal potassium isotopic abundances [15]. The original data from von Egidy *et al.* [12] and Krusche *et al.* [13,14] were normalized assuming the total observed intensity feeding the GS is 100. Weak transitions not observed in our work but seen in the earlier experiments were renormalized by a least-squares fit to the Budapest cross-section data and used to complete the  $(n, \gamma)$  level schemes.

### III. SIMULATION OF THE NEUTRON CAPTURE $\gamma$ -RAY DECAY SCHEME

The contribution to the cross section of a large number of transitions feeding the ground state, which are too weak to be observed experimentally, can be estimated from simulations based on a statistical model of the  $\gamma$ -ray decay. Here it is assumed that the microscopic effects of nuclear structure can be ignored, especially for level energies near the neutron separation energy.

#### A. Statistical model simulations

Theoretical feedings of low-lying levels by thermal neutron radiative capture were calculated using the computer code DICEBOX [6]. The algorithm of this Monte Carlo code is based on the generalization of the extreme statistical model, embodying Bohr's idea of a compound nucleus [16]. Below a certain critical energy  $E_{\text{crit}}$  the level scheme, i.e., energies, spins, and parities of all levels as well as all deexciting transitions, is taken from the experiment. In addition, the intensities of the primary transitions' feeding levels below  $E_{\text{crit}}$  are taken from the experiment. This is important as it strongly eliminates the possible influence of direct neutron capture, which does not follow the rules of the statistical approach. Above  $E_{\text{crit}}$ , a set of levels is generated as a random discretization of an *a priori* known level density formula  $\rho(E, J^\pi)$ . The decay properties of an initial level  $i$  above  $E_{\text{crit}}$  are completely characterized by a full set of partial radiation widths to all final levels  $f$  below the level  $i$ . A partial radiative width  $\Gamma_{i\gamma f}$ , which characterizes the probability of  $\gamma$ -ray decay with an energy  $E_\gamma = E_i - E_f$ , is assumed to be a random choice from the Porter-Thomas distribution [17] with a mean value

$$\langle \Gamma_{i\gamma f} \rangle = \frac{f^{(XL)}(E_\gamma, \xi) \times E_\gamma^3}{\rho(E_i, J_i^\pi)}. \quad (1)$$

Here  $\rho(E_i, J_i^\pi)$  is the level density near the initial level  $i$  and  $f^{(XL)}(E_\gamma, \xi)$  is the photon strength function (PSF) for a transition of given type  $X$  and multipolarity  $L$ . Only  $E1$ ,  $M1$ , and  $E2$  transitions were considered. The argument  $\xi$  of the PSF represents a possible dependence on quantities other than  $\gamma$ -ray energy. In the extreme statistical model it is assumed that individual  $\Gamma_{i\gamma f}$  are independent and uncorrelated. The selection rules for different types of transitions are fully accounted for in the generation of  $\Gamma_{i\gamma f}$ .

The random generation of a system of all  $\Gamma_{i\gamma f}$ , which fully describes the decay properties of all nuclear levels above  $E_{\text{crit}}$ , is called a *nuclear realization*. Due to the fluctuations involved there exists an infinite number of nuclear realizations that differ in decay properties even for a single choice of  $f^{(XL)}$  and level density. Consequently, all simulated quantities are subject to statistical fluctuations arising from different nuclear realizations. The determination of these fluctuations with the DICEBOX code allows us to estimate the uncertainty coming from the statistical nature of the decay process. Typically a calculation consisted of 50 nuclear realizations, each with 50 000 capture state decays, generated by the Monte Carlo method. DICEBOX stores the simulated capture state deexcitation data, which are used to calculate populations of

low-lying levels below  $E_{\text{crit}}$  and intensities of all  $\gamma$  rays per neutron capture. Simulated intensities can be renormalized to absolute cross sections by comparison with the experimental  $\gamma$ -ray cross sections depopulating the low-lying levels.

The energy dependence and absolute values of  $f^{(XL)}(E_\gamma, \xi)$  are not sufficiently known for nuclei with  $A \lesssim 50$ . We therefore have used only simple models for these quantities in our simulations. For  $E1$  transitions we adopted three different models: (i) the Lorentzian shape of Giant Dipole Electric Resonance (GDER) [18] in conjunction with the Brink hypothesis [19], also called the standard Lorentzian (SLO) model, (ii) the Kadenskĩ, Markushev, and Furman (KMF) model [20], which modifies the shape of the low-energy tail of GDER, and (iii) the single-particle (SP) model [21,22], where  $f^{(E1)} = \text{const.}$  is independent of  $\gamma$ -ray energy. The parameters of GDER were obtained from a fit to  $^{39}\text{K}(\gamma, n)$  data [23] for energies  $16 \text{ MeV} < E_\gamma < 23 \text{ MeV}$ . The shape of GDER from this fit at energies below about 10 MeV is nearly identical to shapes for  $^{40}\text{Ca}$  and  $^{51}\text{V}$  targets whose GDER parameters can be found in the survey of Dietrich and Berman [24].

For  $M1$  strength two different models were used: (i) the SP model where  $f^{(M1)} = \text{const.}$ , and (ii) a model where  $f^{(M1)}$  is described as a Lorentzian-shaped giant dipole magnetic resonance (GDMR) at about 12 MeV with a width about 4 MeV [25,26]. The strengths of  $f^{(M1)}$  were adjusted to match the observed population of positive and negative parity levels at low excitation energies. For  $E2$  strength a SP model was used although this strength has only a minor impact on the decay of levels at higher excitation energies.

The back-shifted Fermi gas (BSFG) and constant-temperature (CT) models, in the parametrization from Ref. [27], were used for level density. All possible combinations of  $f^{(XL)}$  and level density were tested in these simulations.

## B. Direct neutron capture

In most light nuclei the direct-capture mechanism accounts for a significant part of the thermal-neutron capture cross section [28]. The intensities of primary transitions, especially those to low-lying levels, are expected to be governed by both statistical considerations and direct neutron capture. According to Mughabghab [29] the contribution of the direct neutron capture cross section is expected to be  $\sigma_D = 0.75 \text{ b}$  out of  $\sigma_0 \approx 2.3 \text{ b}$  for  $^{39}\text{K}(n, \gamma)$  and  $\sigma_D = 1.32 \text{ b}$  out of  $\sigma_0 \approx 1.6 \text{ b}$  for  $^{41}\text{K}(n, \gamma)$ . There is no estimate of  $\sigma_D$  for  $^{40}\text{K}(n, \gamma)$  but as  $\sigma_D$  rarely exceeds several barns its contribution to  $\sigma_0 \approx 90 \text{ b}$  for  $^{40}\text{K}$  should be very small.

If direct capture were important the primary transitions, especially in  $^{42}\text{K}$ , could not be treated within a statistical approach using the DICEBOX algorithm. However, the intensities of primary transitions to levels below  $E_{\text{crit}}$  are taken from the experiment in these simulations and are not model dependent. For primary transitions to levels above  $E_{\text{crit}}$  we can compare DICEBOX simulations with the experimental distribution of cumulative intensity of primary transitions as a function of  $\gamma$ -ray energy. A comparison of the experimental distribution with the prediction of simulations based on one model combination of  $f^{(XL)}$  and the level density for  $^{42}\text{K}$  is shown in Fig. 1. Each

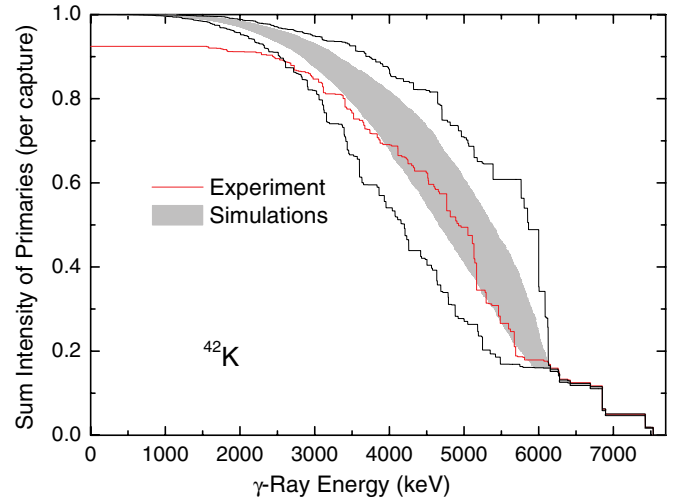


FIG. 1. (Color online) Cumulative distribution of primary transitions in  $^{42}\text{K}$ . Simulated intensities for  $E_\gamma > 6.1 \text{ MeV}$  were taken from experiment. Simulations were made with SLO model for  $E1$ , SP for  $M1$ , and BSFG model for level density. As for simulated values, the lines correspond to minimum and maximum values obtained while the gray region accommodates 68% of all values. The deviation of the experimental value from the simulated one at low  $\gamma$ -ray energies corresponds to the fact that primary transitions with low energies are very weak and escape the detection.

nuclear realization produces a separate curve in the plot and the curves from different nuclear realizations form the expected statistical distribution of primary  $\gamma$  rays. The envelope of this distribution, obtained from the simulation of 100 different nuclear realizations, is shown in Fig. 1 together with a region that contains 68% of all curves.

The experimental data are fully consistent with these statistical model simulations. Similar figures are obtained using various model combinations for all potassium isotopes. This indicates that a possible contribution of direct neutron capture can be completely neglected in simulations of primary transitions to levels above  $E_{\text{crit}}$ . Approximately 85–95% of primary transitions were experimentally observed in the potassium isotopes and the rest are either observed but unplaced transitions feeding the GS or weak transitions that are below the experimental detection limits. As shown in Fig. 1 most of these weak transitions feed levels at high excitation energies above  $\approx 4 \text{ MeV}$ .

## C. Corrections to the observed cross section $\sigma_0$

The experimentally observed cross section feeding the GS must be corrected for unobserved GS transitions to determine  $\sigma_0$ . The relatively low-level density for the potassium isotopes allows the observation of a significant portion of their decay schemes [12–14] including the ground-state transitions from levels up to near the neutron separation energy so this correction is expected to be small. We compared the intensities of individual transitions simulated by the DICEBOX code with the experiment, assuming that all transitions with intensities  $I$  higher than the detection threshold  $I_{\text{thr}}$  were observed and transitions with  $I < I_{\text{thr}}$  were not observed.

We also assumed that the level scheme was essentially complete up to 4 MeV so only unplaced measured  $\gamma$  rays with energies greater than 4 MeV could be possible ground-state transitions. The total intensity of these transitions was assumed to be an upper limit on this contribution so a correction factor  $\sigma_\gamma(E < 4 \text{ MeV})/2$  with an uncertainty of 100% was added to the observed value. These corrections were always small with respect to the total cross section  $\sigma_0$ .

An estimate of the unobserved intensity of transitions feeding the GS has also been done in another way as described in our previous paper [5] where we assumed that  $\sigma_0$  can be written as

$$\sigma_0 = \Sigma\sigma_\gamma^{\text{exp}}(\text{GS}) + \Sigma\sigma_\gamma^{\text{sim}}(\text{GS}), \quad (2)$$

where  $\Sigma\sigma_\gamma^{\text{exp}}(\text{GS})$  is the sum of  $\gamma$ -ray cross sections populating the ground state from the experimentally observed levels below  $E_{\text{crit}}$  and  $\Sigma\sigma_\gamma^{\text{sim}}(\text{GS})$  is the simulated sum of  $\gamma$ -ray cross sections populating the ground state from all levels above  $E_{\text{crit}}$ . As will be shown, both estimates give very consistent results, which supports the use of the statistical approach to the simulation of  $\gamma$  decay from radiative neutron capture for the potassium isotopes. The uncertainty in the cross section based on Eq. (2) is usually much higher than the uncertainty deduced from unobserved transitions, see below.

#### IV. RESULTS

Detailed measurements of the relative  $\gamma$ -ray intensity depopulating the capture state in  $^{40}\text{K}$  were done by von Egidy *et al.* [12] on a natural potassium target, and by Krusche *et al.* [13,14] who measured relative  $\gamma$ -ray intensities depopulating the capture states in  $^{41,42}\text{K}$  using enriched targets. For each isotope nearly 100% of the total  $\gamma$ -ray cross section feeding the ground state was observed. These intensity measurements were renormalized to a cross-section scale by a constant factor  $N = \sigma_\gamma/I_\gamma$  determined by a least-squares fit of the Krusche *et al.* intensities  $I_\gamma$  to the Budapest Reactor cross section  $\sigma_\gamma$  measurements for  $\gamma$  rays common to both experiments. The Budapest Reactor and renormalized von Egidy *et al.* and Krusche *et al.* data were then combined to determine the experimental cross sections populating/depopulating the levels.

The correction for unobserved statistical feeding to the ground state of each isotope was calculated using the DICEBOX simulations assuming a detection threshold for  $\gamma$  transitions. A detection threshold  $I_{\text{thr}}$  was chosen based on the minimum experimental intensity observed by the authors of Refs. [12–14]. Energy-independent threshold intensities  $I_{\text{thr}} = 0.0005\text{--}0.001$  per neutron capture were tested. These values are very close to  $I_{\text{thr}}$  suggested by the authors of Ref. [14] and the experimental data indicate that the energy dependence of this threshold is minimal. These thresholds were applied to  $\gamma$  spectra simulated with all of the combinations of the models for level density and  $f^{(XL)}$  listed above. The results did not depend significantly on the combination of the model of  $f^{(XL)}$  and level density chosen. A slightly stronger dependence on the adopted model combination was obtained if the correction was made using

Eq. (2) as seen in the results for the individual potassium isotopes.

A comparison of the experimental and simulated feeding for individual low-lying levels can be visualized by plotting the experimental depopulation of levels below  $E_{\text{crit}}$  against their simulated populations in population-depopulation (P-D) diagrams. If the simulation was perfect all points in these diagrams would align with the slope giving the normalization of the simulation from the transition intensity per neutron capture to the experimental cross section. Scatter around the line indicates the quality and completeness of both the simulation and the experimental data. Uncertainties in these diagrams along the horizontal axis correspond to experimental errors while those along the vertical axis come from uncertainties due to Porter-Thomas fluctuations while generating partial radiation widths and level energies in different nuclear realizations. All P-D plots shown in this paper were obtained with the model combination SLO( $E1$ ) + SP( $M1$ ) + BSFG. The plots for all other model combinations are similar.

#### A. $^{39}\text{K}(n, \gamma)^{40}\text{K}$

Table II lists 386  $\gamma$  rays that we have assigned to  $^{40}\text{K}$  combining our measurements with those of von Egidy *et al.* [12]. The agreement between our data and that of von Egidy *et al.* is excellent. Only unplaced  $\gamma$  rays that were observed in both experiments are listed in Table II. The  $^{40}\text{K}$  level scheme was constructed by comparison to the work of von Egidy *et al.* and other data compiled in the ENSDF [11] file. Numerous multiple placements of  $\gamma$  rays by von Egidy *et al.* have been resolved in this work on the basis consistency with the level energies, intensity balance through the level scheme, and spin/parity considerations. A total of 79 levels and the capture state are assigned to  $^{40}\text{K}$ .

The low-energy 29.8-keV transition deexciting the first excited state was not directly observed in either the Budapest or von Egidy *et al.* measurements and its intensity in Table II is calculated from the observed experimental cross section populating the level. A least-squares fit to the Budapest and von Egidy *et al.* [12] data gives a normalization factor of  $N = 0.0235 \pm 0.0003$  for converting the  $\gamma$ -ray intensities to the cross-section scale. The experimental cross sections populating and depopulating levels in  $^{40}\text{K}$  are shown in Table III where the total cross section observed feeding the GS and the first excited state at 29.8 keV of  $^{40}\text{K}$  is  $2.252 \pm 0.016$  b. The total energy weighted cross section is  $\Sigma E_\gamma \times I_\gamma = 2.04 \pm 0.03$  b for  $\gamma$  rays placed in the level scheme and  $0.13 \pm 0.02$  b for unplaced transitions. The  $^{40}\text{K}$  level scheme is well studied by various reactions up to about 4 MeV and only one unplaced  $\gamma$  ray with an energy higher than 4 MeV that could feed the GS was found with a cross section 6 mb.

In our previous paper [5] we showed that when two possible capture state spins can contribute to thermal neutron capture the simulated populations of levels with low and high spins will depend on this contribution. Unlike the Pd case, a very weak dependence is seen on the contribution of  $J^\pi = 1^+$  and  $2^+$  resonances in neutron capture on the  $^{39}\text{K}$  target. Primary  $\gamma$ -ray



TABLE II.  $^{39}\text{K}(n, \gamma)$  thermal neutron capture  $\gamma$ -ray energies and cross sections measured in this work are compared with the  $I_\gamma$  and  $E_\gamma$  values from von Egidy *et al.* [12].

This work		von Egidy <i>et al.</i> [12]		Placement	This work		von Egidy <i>et al.</i> [12]		Placement
$E_\gamma$ (keV)	$\sigma_\gamma$ (b) <sup>a</sup>	$E_\gamma$ (keV)	$I_\gamma$ <sup>b</sup>		$E_\gamma$ (keV)	$\sigma_\gamma$ (b) <sup>a</sup>	$E_\gamma$ (keV)	$I_\gamma$ <sup>b</sup>	
29.8299(5)	1.938(15) <sup>c</sup>	29.8299(5)	86.2(69)	30 → 0					892 → 29
106.1(3)	0.00058(4)			2397 → 2290	870.26(6)	0.0036(3)	869.97(4)	0.143(15)	Unplaced
186.02(12)	0.00080(15)	185.97(1)	0.118(19)	2290 → 2104	891.55(3)	0.0213(7)	891.372(21)	0.90(9)	892 → 0
249.54(16)	0.00029(7)			3664 → 3414	903.86(8)	0.0034(3)	903.878(23)	0.150(15)	4744 → 3840
311.26(7)	0.00286(23)	311.13(4)	0.133(15)	2730 → 2419		0.00040(7)	920.12(18)	0.017(3)	4149 → 3229
315.57(10)	0.00176(21)	315.52(8)	0.062(8)	2576 → 2260		0.00045(9)	926.24(15)	0.019(4)	3713 → 2787
	0.00021(12)	320.9(6)	0.009(5)	3128 → 2808		0.00087(9)	946.29(8)	0.037(4)	4744 → 3798
	0.00146(19)	327.23(8)	0.062(8)	2397 → 2070		0.00101(13)	951.16(7)	0.043(5)	4180 → 3229
330.92(4)	0.0069(3)	330.798(7)	0.33(3)	2290 → 1959	958.5(4)	0.0009(3)	958.35(9)	0.026(3)	3028 → 2070
	0.00094(13)	335.44(14)	0.040(6)	3821 → 3486	976.80(13)	0.0029(3)	976.85(6)	0.109(12)	5190 → 4213
	0.00085(14)	337.75(12)	0.036(6)	2757 → 2419	981.14(19)	0.0025(3)	981.03(7)	0.103(12)	3557 → 2576
349.42(11)	0.00117(20)	349.33(4)	0.053( )	2419 → 2070	1023.44(7)	0.0051(3)	1023.21(4)	0.26(3)	3599 → 2576
371.87(6)	0.00404(25)	371.792(10)	0.172(18)	3128 → 2757	1027.1(4)	0.0012(3)	1027.09(24)	0.036(8)	2986 → 1959
382.98(20)	0.00095(21)	383.01(18)	0.020(4)	3798 → 3414		0.00089(16)	1034.28(20)	0.038(6)	4021 → 2986
	0.00070(18)	397.28(17)	0.030(7)	3154 → 2757	1058.08(17)	0.0024(3)	1058.03(4)	0.112(12)	4544 → 3486
453.84(21)	0.00069(18)	454.19(8)	0.038(5)	3869 → 3414	1062.5(3)	0.0019(3)	1062.20(8)	0.052(6)	3109 → 2047
460.22(5)	0.00412(23)	460.092(14)	0.136(15)	2419 → 1959	1068.91(6)	0.0089(5)	1068.87(3)	0.40(4)	3028 → 1959
496.01(16)	0.00115(27)	496.06(4)	0.047(5)	2787 → 2291	1074.24(15)	0.0029(3)	1074.39(9)	0.144(17)	3821 → 2747
522.41(3)	0.0391(8)	522.319(7)	1.53(16)	2626 → 2104	1078.6(3)	0.0016(3)	1079.44(13)	0.100(13)	4473 → 3394
	0.00040(7)	528.76(14)	0.017(3)	3557 → 3028	1082.74(13)	0.0038(5)	1082.92(7)	0.200(22)	4111 → 3028
	0.00021(7)	534.3(3)	0.009(3)	4021 → 3486	1086.70(4)	0.0250(8)	1086.707(19)	1.11(11)	2730 → 1644
554.83(8)	0.0034(3)	554.74(23)	0.133(17)	3664 → 3109		0.00087(22)	1090.9(3)	0.037(9)	3821 → 2730
563.72(24)	0.0010(3)	563.86(6)	0.073(9)	4744 → 4180		0.00099(14)	1100.13(18)	0.042(6)	4254 → 3154
570.00(13)	0.0027(3)	569.98(7)	0.062(8)	Unplaced	1112.9(3)	0.0013(3)	1113.3(3)	0.029(5)	2757 → 1644
	0.00080(15)	602.96(7)	0.034(6)	3630 → 3028	1118.2(7)	0.0009(3)	1118.38(13)	0.054(7)	4104 → 2986
613.31(6)	0.0053(3)	613.384(24)	0.203(23)	3599 → 2986	1121.63(19)	0.0021(3)	1121.77(7)	0.111(12)	3869 → 2747
627.72(8)	0.00250(28)	627.66(3)	0.095(10)	3414 → 2787	1124.74(18)	0.0019(3)	1124.91(6)	0.120(13)	4111 → 2986
640.42(21)	0.0018(3)	640.4(6)	0.044(22)	3869 → 3229	1130.76(25)	0.0014(3)	1131.17(5)	0.103(11)	3888 → 2757
646.271(25)	0.0508(9)	646.223(5)	2.10(12)	2290 → 1644	1144.42(22)	0.0016(3)	1144.7(5)	0.08(3)	4744 → 3599
657.40(16)	0.00137(23)	657.39(3)	0.078(8)	3414 → 2757	1150.60(13)	0.0042(5)	1150.58(18)	0.23(4)	3109 → 1959
666.69(12)	0.00198(24)	666.91(5)	0.057(6)	2626 → 1959	1158.88(24)	0.180(3)	1158.901(20)	7.8(8)	1959 → 800
	0.00064(13)	678.13(20)	0.027(5)	3486 → 2808	1162.21(10)	0.0061(5)	1162.59(24)	0.31(5)	4149 → 2986
695.32(23)	0.00125(23)	695.31(8)	0.042(6)	2986 → 2291	1178.15(13)	0.0078(9)	1178.38(4)	0.36(4)	2070 → 891
	0.00033(6)	727.1(3)	0.014(3)	4213 → 3486	1187.27(16)	0.0025(3)	1187.45(8)	0.062(7)	3146 → 1959
	0.00056(10)	730.48(15)	0.024(4)	3840 → 3109	1195.70(24)	0.0014(3)	1195.81(7)	0.055(6)	3486 → 2291
737.51(10)	0.0036(3)	737.45(3)	0.146(15)	3028 → 2290	1201.95(18)	0.0025(3)	1201.86(5)	0.106(11)	3599 → 2397
740.95(6)	0.0064(3)	740.89(6)	0.26(3)	4180 → 3439		0.00108(14)	1204.36(10)	0.046(6)	4315 → 3146
	0.0019(9)	756.4(6)	0.08(4)	3154 → 2397	1212.94(25)	0.0011(3)	1213.53(8)	0.047(5)	4021 → 2807
	0.0028(10)	760.6(4)	0.12(4)	2808 → 2047	1221.64(24)	0.0017(3)	1221.71(7)	0.067(7)	3798 → 2576
770.325(23)	1.017(14)	770.3053(18)	42.9(39)	800 → 30	1226.13(25)	0.0016(3)	1226.31(5)	0.071(8)	Unplaced
791.16(4)	0.0117(5)	791.06(4)	0.50(5)	Unplaced	1232.59(11)	0.0034(3)	1232.74(3)	0.134(14)	3630 → 2397
	0.00146(15)	798.8(3)	0.062(7)	4213 → 3414	1247.20(3)	0.0883(15)	1247.173(24)	3.8(4)	2047 → 800
799.84(13)	0.0029(3)	800.3(3)	0.063(7)	800 → 0	1255.29(14)	0.0024(3)	1255.29(9)	0.107(12)	5024 → 3769
	0.00054(9)	811.39(13)	0.023(4)	3798 → 2986	1262.1(3)	0.0016(3)			3888 → 2626
812.88(17)	0.0013(3)	813.12(7)	0.046(6)	4993 → 4180		0.0025(5)	1267.5(3)	0.105(21)	4396 → 3128
827.58(4)	0.0109(5)	827.552(15)	0.45(5)	2787 → 1959	1269.68(6)	0.0081(5)	1269.56(5)	0.47(5)	2070 → 800
838.31(20)	0.00107(23)	838.8(5)	0.066(17)	3128 → 2290	1282.8(4)	0.0009(3)	1283.3(3)	0.051(16)	Unplaced
843.50(4)	0.0222(6)	843.478(16)	1.57(16)	1644 → 800	1303.42(3)	0.0619(14)	1303.53(7)	2.7(3)	2104 → 800
848.59(10)	0.00218(25)	848.7(3)	0.104(19)	2808 → 1959	1308.96(25)	0.0018(3)	1308.9(4)	0.043(17)	3599 → 2290
1320.81(9)	0.0074(6)	1320.9(4)	0.30(3)	3368 → 2047	1795.36(4)	0.0329(9)	1795.45(4)	1.34(14)	3439 → 1644
1331.59(19)	0.0028(5)	1331.58(4)	0.152(16)	Unplaced		0.00169(22)	1813.94(14)	0.072(9)	4104 → 2291
	0.00078(13)	1335.48(18)	0.033(6)	3439 → 2104	1820.11(11)	0.0057(6)	1820.35(5)	0.27(3)	4396 → 2576
1348.2(5)	0.0008(5)	1348.06(14)	0.035(4)	3924 → 2576	1825.60(6)	0.0166(8)	1825.77(5)	0.65(7)	2626 → 800
1354.21(15)	0.0039(5)	1354.12(3)	0.161(7)	4111 → 2757	1831.54(22)	0.0032(6)	1832.01(5)	0.117(12)	4960 → 3128
1365.2(3)	0.0016(3)	1365.06(24)	0.066(12)	4351 → 2986	1838.48(8)	0.0106(7)	1838.61(8)	0.44(4)	3798 → 1959
1373.20(4)	0.0283(8)	1373.227(21)	1.29(13)	3664 → 2291	1846.25(19)	0.0026(6)	1846.72(6)	0.105(11)	4993 → 3146
1392.8(4)	0.0021(5)	1393.16(8)	0.126(14)	5190 → 3798	1854.87(21)	0.0034(5)	1854.99(5)	0.202(21)	Unplaced
1399.06(6)	0.0117(6)	1399.03(4)	0.53(5)	2291 → 891	1858.42(7)	0.0122(6)	1858.51(5)	0.54(5)	4149 → 2291
1402.80(16)	0.0033(7)	1402.73(9)	0.125(14)	4960 → 3557	1881.16(8)	0.0104(6)	1881.20(5)	0.50(5)	3840 → 1959
1418.78(13)	0.0034(5)	1419.01(3)	0.233(24)	Unplaced	1888.5(4)	0.0017(6)	1888.43(8)	0.098(11)	4149 → 2260
1424.12(8)	0.0078(6)	1424.229(23)	0.36(4)	3821 → 2397	1910.49(18)	0.0037(5)	1910.70(6)	0.171(18)	Unplaced
	0.00052(8)	1427.45(18)	0.022(3)	4537 → 3109	1916.29(16)	0.0043(5)	1916.51(6)	0.26(3)	4020 → 2104

TABLE II. (Continued.)

This work		von Egidy <i>et al.</i> [12]		Placement	This work		von Egidy <i>et al.</i> [12]		Placement
$E_\gamma$ (keV)	$\sigma_\gamma$ (b) <sup>a</sup>	$E_\gamma$ (keV)	$I_\gamma$ <sup>b</sup>		$E_\gamma$ (keV)	$\sigma_\gamma$ (b) <sup>a</sup>	$E_\gamma$ (keV)	$I_\gamma$ <sup>b</sup>	
1434.35(19)	0.0024(5)	1434.50(6)	0.140(15)	3394 → 1959	1919.28(20)	0.0035(5)			4180 → 2260
1438.59(9)	0.0055(5)	1438.72(4)	0.218(23)	3486 → 2047	1929.18(6)	0.0447(10)	1929.32(10)	1.8(3)	1959 → 30
	0.00047(5)	1452.39(12)	0.0200(20)	3713 → 2261		0.012(7)	1930.2(3)	0.5(3)	2730 → 800
1460.25(19)	0.0025(5)	1460.81(10)	0.049(6)	Unplaced	1931.23(20)	0.0075(6)			5489 → 3557
1466.09(10)	0.0053(5)	1466.11(3)	0.26(3)	3109 → 1644	1953.5(3)	0.0051(6)	1953.74(6)	0.31(3)	5063 → 3110
1477.83(25)	0.0041(9)	1478.01(6)	0.32(3)	3738 → 2260	1956.49(5)	0.0457(12)	1956.58(5)	1.84(18)	2757 → 800
1479.87(5)	0.0398(10)	1480.09(4)	1.54(16)	3439 → 1959	1961.29(20)	0.0037(6)	1961.11(6)	0.154(16)	4537 → 2576
1484.1(4)	0.0011(5)	1483.86(8)	0.077(9)	Unplaced		0.00087(15)	1964.27(23)	0.037(6)	3924 → 1960
	0.0023(4)	1487.42(9)	0.097(12)	4473 → 2986	1973.14(9)	0.0070(6)	1973.00(4)	0.32(3)	4020 → 2047
1489.62(4)	0.0312(9)	1489.77(5)	1.21(12)	2290 → 800	1994.08(19)	0.0035(6)	1994.08(15)	0.188(24)	Unplaced
1496.0(3)	0.0012(5)			3599 → 2104	2000.8(3)	0.0020(5)	2001.24(20)	0.201(23)	4104 → 2103
1502.79(7)	0.0096(6)	1503.00(10)	0.41(4)	3146 → 1644	2007.71(4)	0.0578(14)	2007.71(7)	2.5(3)	2808 → 800
	0.00052(9)	1509.9(3)	0.022(4)	3154 → 1644		0.0040(7)	2013.90(20)	0.17(3)	4744 → 2730
1516.83(18)	0.0020(3)	1517.10(9)	0.122(4)	Unplaced	2017.49(4)	0.0608(14)	2017.53(4)	2.7(3)	2047 → 30
1537.16(12)	0.0039(5)	1536.84(5)	0.26(3)	3798 → 2260	2022.37(18)	0.0043(6)	2022.32(17)	0.165(23)	4419 → 2397
1551.65(14)	0.0034(5)	1551.77(9)	0.102(12)	3599 → 2047	2039.94(4)	0.0585(15)	2039.94(4)	2.7(3)	2070 → 30
1560.7(4)	0.0030(7)	1560.44(19)	0.175(21)	3630 → 2070	2047.33(4)	0.0605(15)	2047.28(4)	2.7(3)	2047 → 0
	0.00082(10)	1578.97(12)	0.035(4)	3869 → 2290	2056.8(3)	0.0025(5)	2057.07(5)	0.141(16)	4104 → 2047
1566.27(24)	0.0029(6)	1566.21(7)	0.155(17)	4960 → 3394	2069.75(5)	0.0409(11)	2070.08(15)	2.01(20)	2070 → 0
1597.71(7)	0.0063(3)	1597.88(4)	0.29(3)	3888 → 2290	2073.67(4)	0.155(3)	2073.74(10)	6.5(7)	2104 → 30
1613.76(3)	0.1345(23)	1613.84(4)	5.7(6)	1644 → 30	2077.41(13)	0.0078(6)			4808 → 2730
1618.98(3)	0.1461(24)	1619.00(4)	6.2(6)	2419 → 800		0.00113(12)	2094.61(10)	0.048(5)	3738 → 1644
1625.70(8)	0.0077(5)	1625.67(14)	0.32(4)	4251 → 2626	2109.9(3)	0.0015(5)			4180 → 2070
1634.26(8)	0.0065(5)			3924 → 2290		0.00073(10)	2115.77(14)	0.031(4)	4873 → 2757
1665.44(22)	0.0032(5)	1665.43(4)	0.143(15)	4396 → 2730	2121.6(3)	0.0018(5)	2122.02(5)	0.121(3)	Unplaced
1668.1(3)	0.0024(5)	1667.69(5)	0.102(11)	Unplaced	2143.2(3)	0.0025(5)	2143.37(11)	0.139(16)	4213 → 2070
	0.0024(7)	1680.8(4)	0.10(3)	4667 → 2986	2149.90(14)	0.0083(6)	2149.93(5)	0.43(4)	4254 → 2104
1690.91(24)	0.0017(5)	1691.26(6)	0.111(12)	3738 → 2047	2153.70(7)	0.0178(8)	2153.81(4)	0.79(8)	3798 → 1644
	0.0024(3)	1695.44(8)	0.100(11)	5063 → 3368	2168.18(15)	0.0043(5)	2168.16(4)	0.179(19)	4744 → 2576
1702.22(15)	0.0054(5)	1702.35(3)	0.33(3)	6097 → 4396	2173.43(18)	0.0032(5)	2173.67(8)	0.094(10)	4960 → 2786
1704.76(5)	0.0275(9)	1704.70(20)	0.31(16)	Multiple <sup>d</sup>	2184.41(5)	0.0223(8)	2183.70(20)	0.47(24)	4254 → 2070
1717.99(20)	0.0024(5)	1718.68(4)	0.166(7)	4873 → 3154		0.011(6)	2185.70(20)	0.47(24)	2986 → 800
1751.66(14)	0.0045(5)	1751.76(5)	0.225(23)	4149 → 2397	2196.40(9)	0.0086(6)	2196.61(5)	0.34(4)	3840 → 1644
	0.00085(13)	1754.72(17)	0.036(5)	3713 → 1959	2203.88(23)	0.0062(7)	2204.08(10)	0.34(4)	4960 → 2756
	0.00070(10)	1761.10(17)	0.030(4)	4180 → 2419	2206.27(10)	0.0187(14)	2206.35(10)	0.75(8)	4254 → 2047
1765.20(12)	0.0054(5)	1765.24(15)	0.224(23)	3869 → 2104		0.0043(6)	2221.27(11)	0.183(24)	4180 → 1959
1779.14(8)	0.0077(5)			3738 → 1959	2230.58(6)	0.0228(11)	2230.54(5)	0.81(8)	2260 → 30
	0.004(4)	2233.0(4)	0.16(16)	4281 → 2047	2736.01(9)	0.0130(8)	2736.09(9)	0.83(5)	7800 → 5063
2246.3(3)	0.0034(6)			4350 → 2104	2747.4(3)	0.0034(6)	2747.00(18)	0.26(3)	2747 → 0
2260.17(10)	0.0078(6)	2260.11(10)	0.31(3)	2260 → 0	2756.63(7)	0.0307(11)	2756.81(7)	1.93(10)	2787 → 30
2271.1(3)	0.0017(3)	2271.19(12)	0.085(10)	Unplaced	2775.12(21)	0.0038(6)	2775.21(17)	0.27(3)	7800 → 5024
2290.64(5)	0.0655(15)	2290.58(7)	2.8(3)	2291 → 0	2785.53(22)	0.0044(6)	2784.4(4)	0.21(5)	4744 → 1959
2310.70(10)	0.0102(7)	2310.70(5)	0.51(5)	7800 → 5489		0.0033(12)	2787.0(6)	0.14(5)	2787 → 0
2323.1(3)	0.0021(5)	2322.75(13)	0.127(14)	Unplaced	2799.20(8)	0.0163(8)	2799.30(18)	0.95(10)	3599 → 800
2330.54(16)	0.0051(6)	2330.16(10)	0.28(3)	Unplaced	2806.35(7)	0.0288(10)	2806.53(12)	1.76(13)	7800 → 4993
2346.22(11)	0.0155(8)	2346.05(10)	0.69(7)	3146 → 800	2839.52(7)	0.0322(10)	2839.71(7)	1.87(10)	7800 → 4960
2348.89(22)	0.0054(6)	2348.72(9)	0.24(3)	4396 → 2047	2856.85(14)	0.0063(6)	2857.15(15)	0.29(3)	4960 → 2103
2359.8(8)	0.0008(5)			5489 → 3128	2892.01(14)	0.0071(6)	2892.19(15)	0.36(3)	4850 → 1959
2367.18(7)	0.0177(8)	2367.17(5)	0.58(6)	2397 → 30	2912.30(23)	0.0037(6)	2912.6(3)	0.145(21)	4960 → 2047
2374.90(16)	0.0074(6)	2373.74(5)	0.102(11)	Unplaced	2917.65(10)	0.0148(8)	2917.81(9)	0.89(5)	Unplaced
	0.0027(3)	2375.85(5)	0.113(12)	4667 → 2291	2922.50(19)	0.0068(7)	2922.91(20)	0.33(3)	4993 → 2070
2383.80(21)	0.0042(5)	2384.99(11)	0.141(15)	Unplaced	2926.54(12)	0.0116(8)	2926.85(10)	0.73(5)	7800 → 4873
2389.27(6)	0.0339(11)	2389.18(5)	1.34(13)	2419 → 30	2938.42(11)	0.0109(7)	2938.32(9)	0.67(4)	3738 → 800
2393.7(4)	0.0026(6)	2393.84(12)	0.108(12)	4464 → 2070	2949.08(11)	0.0099(7)	2949.23(15)	0.63(4)	7800 → 4850
2397.25(17)	0.0061(6)	2397.12(6)	0.224(23)	2397 → 0	2955.76(17)	0.0056(6)	2955.94(16)	0.41(3)	2986 → 30
2403.06(21)	0.0038(6)	2403.04(9)	0.119(13)	5190 → 2786	2967.6(3)	0.0027(5)	2967.8(3)	0.163(19)	3768 → 800
	0.0046(5)	2416.06(11)	0.194(23)	4464 → 2047	2992.41(16)	0.0073(8)	2992.60(14)	0.50(3)	7800 → 4808
2418.27(10)	0.0158(8)	2418.69(15)	0.63(6)	2419 → 0	3010.29(12)	0.0079(8)	3010.55(14)	0.50(3)	7800 → 4789
2424.62(12)	0.0123(8)	2424.66(5)	0.54(6)	Unplaced	3027.8(3)	0.0027(6)	3027.7(3)	0.139(18)	3028 → 0
	0.0059(8)	2428.28(9)	0.25(3)	3229 → 800	3034.34(14)	0.0077(6)	3034.43(17)	0.293(24)	4993 → 1959
	0.00059(8)	2454.7(3)	0.025(4)	4744 → 2290	3039.93(11)	0.0101(7)	3040.24(13)	0.62(4)	3840 → 800
2459.65(16)	0.0041(5)	2459.48(5)	0.191(20)	5190 → 2730	3055.30(7)	0.0523(14)	3055.58(12)	2.86(17)	7800 → 4744

TABLE II. (Continued.)

This work		von Egidy <i>et al.</i> [12]		Placement	This work		von Egidy <i>et al.</i> [12]		Placement
$E_\gamma$ (keV)	$\sigma_\gamma$ (b) <sup>a</sup>	$E_\gamma$ (keV)	$I_\gamma$ <sup>b</sup>		$E_\gamma$ (keV)	$\sigma_\gamma$ (b) <sup>a</sup>	$E_\gamma$ (keV)	$I_\gamma$ <sup>b</sup>	
2468.2(6)	0.0011(5)	2467.3(10)	0.067(7)	4111 → 1644	3068.32(17)	0.0051(6)	3068.7(4)	0.25(4)	3869 → 800
	0.00086(22)	2483.8(3)	0.029(8)	4744 → 2260	3088.0(3)	0.0038(7)	3088.3(5)	0.19(4)	3888 → 800
	0.0033(4)	2528.44(11)	0.139(15)	4789 → 2260	3098.81(14)	0.0143(8)	3098.56(20)	0.37(14)	3128 → 30
2539.98(23)	0.0041(5)	2539.87(7)	0.27(3)	6097 → 3557		0.009(3)	3100.42(20)	0.37(14)	4744 → 1644
2542.99(23)	0.0099(6)	2542.92(6)	0.77(8)	Unplaced	3127.92(13)	0.0093(6)	3128.06(13)	0.61(4)	3128 → 0
2545.92(6)	0.0604(14)	2545.85(10)	2.8(3)	2576 → 30	3133.05(17)	0.0075(6)	3133.49(14)	0.51(4)	7800 → 4667
	0.00047(7)	2552.64(17)	0.020(3)	7800 → 5247	3137.3(4)	0.0024(5)			7800 → 4662
	0.00078(13)	2568.8(4)	0.033(6)	4213 → 1644	3143.94(19)	0.0046(5)	3144.30(19)	0.28(3)	5214 → 2070
2577.86(11)	0.0059(6)	2577.63(10)	0.32(3)	4537 → 1959	3153.43(22)	0.0044(5)	3153.5(3)	0.38(3)	3154 → 0
	0.0022(3)	2586.06(14)	0.094(11)	7800 → 5214	3198.42(24)	0.0034(5)	3198.6(3)	0.146(22)	3229 → 30
2593.37(9)	0.0109(6)	2593.32(10)	0.50(5)	3394 → 800	3204.6(4)	0.0021(5)	3204.7(4)	0.101(20)	Unplaced
2604.6(3)	0.0021(3)	2604.0(4)	0.12(3)	Unplaced	3213.63(25)	0.0048(5)	3214.12(24)	0.223(24)	Unplaced
2610.00(6)	0.0240(8)	2609.98(9)	1.40(9)	7800 → 5190	3220.03(19)	0.0055(6)	3220.08(21)	0.24(3)	4020 → 800
2614.12(7)	0.0186(7)	2614.21(9)	1.16(7)	3414 → 800	3228.8(4)	0.0024(5)	3229.4(4)	0.132(32)	3229 → 0
2628.4(4)	0.0012(3)	2627.7(3)	0.18(3)	5024 → 2397	3255.72(15)	0.0066(6)	3255.9(4)	0.37(7)	7800 → 4544
2639.00(7)	0.0162(7)	2638.93(11)	1.04(7)	3439 → 800	3262.23(7)	0.0423(12)	3262.56(12)	2.43(17)	7800 → 4537
2643.6(3)	0.0032(5)	2644.0(3)	0.26(4)	5063 → 2419	3304.02(9)	0.0164(8)	3304.24(11)	0.99(7)	4104 → 800
2668.9(3)	0.0019(5)	2668.8(4)	0.107(20)	4960 → 2291	3310.2(3)	0.0026(5)	3310.9(5)	0.12(3)	4111 → 800
2680.9(3)	0.0024(6)	2680.4(5)	0.073(19)	5489 → 2808	3326.29(10)	0.0141(8)	3326.44(12)	0.79(6)	7800 → 4473
2685.95(24)	0.0045(8)	2685.6(3)	0.24(5)	3486 → 801	3335.62(14)	0.0184(15)	3336.3(10)	1.7(8)	7800 → 4464
2688.6(4)	0.0021(7)	2688.1(4)	0.19(5)	5111 → 2424	3338.2(3)	0.0056(14)			3368 → 30
2702.36(23)	0.0041(7)	2702.60(16)	0.28(3)	4993 → 2291	3348.77(9)	0.0194(9)	3348.91(10)	1.12(7)	4149 → 800
2716.77(13)	0.0088(7)	2716.95(11)	0.50(4)	2747 → 30	3368.8(4)	0.0021(5)	3368.9(6)	0.10(3)	3368 → 0
2726.48(8)	0.0253(10)	2726.62(7)	1.58(9)	2757 → 30	3379.45(25)	0.0044(6)	3380.3(4)	0.22(4)	7800 → 4419
2736.01(9)	0.0130(8)	2736.09(9)	0.83(5)	7800 → 5063	3384.52(17)	0.0070(7)	3384.66(24)	0.40(5)	3414 → 30
3403.12(11)	0.0188(9)	3403.59(11)	1.00(7)	7800 → 4396	4135.58(9)	0.0634(19)	4135.58(5)	3.41(18)	7800 → 3664
3418.5(6)	0.0019(6)			5489 → 2070	4169.30(11)	0.0134(8)	4169.31(9)	0.71(4)	7800 → 3630
3448.8(5)	0.0078(18)			7800 → 4351	4200.04(10)	0.0448(16)	4200.04(5)	2.23(12)	7800 → 3599
3452.4(15)	0.0278(16)	3452.2(10)	1.71(10)	4254 → 800	4223.52(14)	0.0141(9)	4223.66(7)	0.83(5)	4254 → 30
3480.4(4)	0.0015(9)	3480.6(5)	0.13(3)	4281 → 800	4242.37(16)	0.0092(9)	4242.47(11)	0.45(3)	7800 → 3557
3518.71(9)	0.0209(10)	3518.85(10)	1.05(7)	7800 → 4281	4280.45(17)	0.0071(5)	4280.35(22)	0.37(4)	4281 → 0
3527.01(11)	0.0191(10)	3526.99(10)	1.02(7)	3557 → 30	4312.71(21)	0.0055(5)	4312.8(3)	0.28(4)	7800 → 3486
3545.64(9)	0.0840(20)	3545.95(6)	4.7(3)	7800 → 4254	4319.6(5)	0.0016(3)			4351 → 30
3548.8(4)	0.0068(18)			7800 → 4251	4360.22(9)	0.0874(24)	4360.19(6)	4.33(24)	7800 → 3439
3569.19(16)	0.0082(7)	3569.30(8)	0.45(3)	3599 → 30	4384.99(12)	0.0278(12)	4384.95(7)	1.48(8)	7800 → 3414
3586.78(25)	0.0038(6)	3586.53(13)	0.217(17)	7800 → 4213	4389.4(3)	0.0057(8)	4389.32(18)	0.37(3)	5190 → 800
3599.5(3)	0.0033(6)	3599.62(20)	0.185(19)	3599 → 0	4405.44(23)	0.0073(8)	4405.36(11)	0.42(3)	7800 → 3394
3619.46(11)	0.0146(9)	3619.40(6)	0.77(4)	7800 → 4180	4421.0(3)	0.0056(7)	4421.15(14)	0.294(22)	Unplaced
3629.82(24)	0.0071(7)	3629.94(15)	0.33(3)	3630 → 0	4431.2(3)	0.0105(9)	4431.17(16)	0.59(5)	7800 → 3368
3633.83(14)	0.0105(8)	3633.88(9)	0.63(4)	3664 → 30	4472.95(17)	0.0074(5)	4472.80(11)	0.40(3)	4473 → 0
3650.25(9)	0.0400(15)	3650.34(5)	2.22(11)	7800 → 4149	4507.16(14)	0.0179(10)	4506.96(7)	0.77(5)	4537 → 30
3663.29(20)	0.0070(7)	3663.32(9)	0.44(3)	4464 → 800	4653.18(17)	0.0124(8)	4652.94(8)	0.52(3)	7800 → 3146
3683.3(5)	0.0024(6)			3713 → 30	4662.1(3)	0.0050(6)			4662 → 0
3688.69(9)	0.0311(12)	3688.67(15)	1.49(12)	7800 → 4111		0.0026(5)	4667.0(4)	0.110(21)	4667 → 0
3695.05(10)	0.0260(11)	3695.15(11)	1.43(10)	7800 → 4104	4670.91(16)	0.0190(10)	4670.84(10)	0.66(4)	7800 → 3128
3736.96(9)	0.0217(7)	3737.01(10)	1.14(7)	4537 → 800	4687.6(4)	0.0018(5)	4688.9(5)	0.052(11)	7800 → 3109
3743.19(23)	0.0029(5)	3743.2(3)	0.21(3)	4544 → 800		0.00179(24)	4842.8(4)	0.076(12)	4873 → 30
3765.1(3)	0.0035(6)	3764.84(19)	0.180(17)	Unplaced	4850.9(8)	0.0020(7)	4851.16(25)	0.120(13)	4850 → 0
3778.66(11)	0.0161(8)	3778.99(10)	0.93(6)	7800 → 4021		0.0059(6)	4872.47(14)	0.252(19)	4873 → 0
3791.4(3)	0.0037(6)	3791.9(3)	0.18(3)	3821 → 30	4929.7(3)	0.0028(5)	4929.3(3)	0.183(21)	4960 → 30
3821.8(3)	0.0052(6)	3822.17(13)	0.264(19)	3821 → 0		0.0025(5)	4962.2(4)	0.107(19)	4993 → 30
3838.47(14)	0.0126(8)	3838.50(7)	0.62(4)	3869 → 30	4991.57(12)	0.0487(16)	4991.38(5)	2.18(11)	7800 → 2808
3857.79(25)	0.0054(6)	3857.97(11)	0.305(21)	3888 → 30	5012.54(13)	0.0255(12)	5012.47(6)	1.17(6)	7800 → 2787
	0.0028(11)	3868.3(4)	0.12(5)	3869 → 0	5042.64(13)	0.0395(17)	5042.43(6)	1.78(9)	7800 → 2757
3874.64(19)	0.0090(7)	3874.7(3)	0.28(6)	7800 → 3924		0.00164(21)	5062.9(4)	0.070(9)	5063 → 0
	0.0049(25)	3895.7(11)	0.21(11)	3924 → 30	5068.82(14)	0.0252(14)	5068.65(6)	1.25(7)	7800 → 2730
3897.81(24)	0.0078(8)	3899.0(7)	0.32(11)	Unplaced	5111.5(7)	0.0019(5)			5111 → 0
3911.37(12)	0.0189(10)	3911.49(18)	0.96(9)	7800 → 3888	5173.33(13)	0.0454(17)			7800 → 2626
3930.68(10)	0.0310(12)	3930.64(5)	1.56(8)	7800 → 3869		0.00125(14)	5188.8(3)	0.053(6)	5190 → 0
3943.94(11)	0.0195(10)	3943.81(6)	0.98(5)	4744 → 800		0.00047(10)	5216.9(6)	0.020(4)	5247 → 30
3959.19(10)	0.0284(11)	3959.19(5)	1.48(8)	7800 → 3840	5222.3(4)	0.0099(9)	5223.14(7)	0.377(20)	7800 → 2576
3977.84(10)	0.0247(11)	3977.83(5)	1.29(7)	7800 → 3821	5379.96(12)	0.164(5)	5379.84(6)	7.9(4)	7800 → 2419
3989.0(3)	0.0038(6)	3989.07(14)	0.242(19)	4789 → 800	5488.5(5)	0.0033(6)			5489 → 0

TABLE II. (Continued.)

This work		von Egidy <i>et al.</i> [12]		Placement	This work		von Egidy <i>et al.</i> [12]		Placement
$E_\gamma$ (keV)	$\sigma_\gamma$ (b) <sup>a</sup>	$E_\gamma$ (keV)	$I_\gamma$ <sup>b</sup>		$E_\gamma$ (keV)	$\sigma_\gamma$ (b) <sup>a</sup>	$E_\gamma$ (keV)	$I_\gamma$ <sup>b</sup>	
4001.78(10)	0.0296(12)	4001.78(5)	1.61(9)	7800 → 3798	5509.24(13)	0.0674(21)	5509.12(7)	3.17(16)	7800 → 2290
	0.0033(4)	4008.1(3)	0.139(15)	4808 → 800	5695.45(13)	0.128(3)	5695.38(7)	5.6(3)	7800 → 2104
4031.09(23)	0.0047(5)	4031.58(14)	0.221(17)	7800 → 3769	5729.19(14)	0.0492(20)	5729.21(7)	2.28(12)	7800 → 2070
4060.99(10)	0.0275(11)	4060.92(5)	1.53(8)	7800 → 3738	5751.76(13)	0.122(3)	5751.60(7)	5.5(3)	7800 → 2047
4080.82(23)	0.0066(7)	4080.69(12)	0.325(22)	4111 → 30	6067.2(4)	0.0014(3)	6067.6(3)	0.050(5)	6097 → 30
4086.29(18)	0.0079(8)	4086.13(9)	0.46(3)	7800 → 3713	6998.78(17)	0.0503(23)	6998.77(10)	2.15(11)	7800 → 800
4110.39(20)	0.0075(7)			4111 → 0	7768.89(20)	0.113(5)	7768.75(19)	5.6(3)	7800 → 30

<sup>a</sup>When the energy is not given the cross section is from the renormalized von Egidy *et al.* [12] data.

<sup>b</sup>For a cross-section multiple by  $0.0235 \pm 0.0003$ .

<sup>c</sup>Intensity calculated from the total population of the 30-keV level.

<sup>d</sup>Cross section divided with 0.200(8) b deexciting the 3663.86 level and 0.0075(8) b deexciting the 4250.8 level.

TABLE III. Cross sections populating and depopulating levels in  $^{40}\text{K}$  from the  $(n, \gamma)$  reaction. The  $J^\pi$  values are from the ENSDF [11], except as indicated. The level energies were calculated by a weighted least-squares fit of the  $\gamma$ -ray energies to the level scheme.

Level energy (keV)	$J^\pi$	In (b)	Out (b)	Net <sup>a</sup> (b)	Level energy (keV)	$J^\pi$	In (b)	Out (b)	Net <sup>a</sup> (b)
0	4 <sup>-</sup>	0.314(4)			3797.54(4)	(1 <sup>+</sup> )	0.0326(13)	0.0355 12	0.0029(18)
29.8299(5)	3 <sup>-</sup>	1.938(15)		{2.252(16) <sup>b</sup>	3821.35(5)	2 <sup>-</sup>	0.0247(11)	0.0228 12	-0.0019(16)
800.124(14)	2 <sup>-</sup>	0.992(11)	1.020 13	0.028(17)	3840.16(4)	(1,2 <sup>+</sup> )	0.0318(11)	0.0297 11	-0.0021(16)
891.55(3)	5 <sup>-</sup>	0.0195(11)	0.0216 6	0.0021(12)	3868.67(5)	2 <sup>-</sup>	0.0310(12)	0.0313 17	0.000(2)
1643.608(19)	0 <sup>+</sup>	0.165(4)	0.1567 24	-0.008(4)	3888.17(6)	(1 <sup>-</sup> ,2,3)	0.0189(10)	0.0185 11	0.000(2)
1959.007(18)	2 <sup>+</sup>	0.1638(24)	0.225 3	0.061(4)	3924.15(7)	(1 <sup>-</sup> to 4 <sup>+</sup> )	0.0090(7)	0.014 3	0.005(3)
2047.375(20)	2 <sup>-</sup>	0.191(6)	0.2096 25	0.019(6)	4020.56(6)	(0 to 3) <sup>-</sup>	0.0161(8)	0.0147 9	-0.0014(12)
2069.752(23)	3 <sup>-</sup>	0.098(3)	0.1153 21	0.018(3)	4104.35(6)	(1 <sup>-</sup> ,2,3 <sup>-</sup> )	0.0260(11)	0.0235 11	-0.0025(16)
2103.544(22)	1 <sup>-</sup>	0.195(3)	0.217 3	0.022(5)	4110.75(6)	(1 <sup>-</sup> ,2,3)	0.0311(12)	0.0266 14	-0.0045(18)
2260.49(4)	3 <sup>+</sup>	0.0228(14)	0.0306 13	0.0078(19)	4148.93(4)	(2 <sup>-</sup> ,3)	0.0400(15)	0.0508 16	0.0108(22)
2289.856(23)	1 <sup>+</sup>	0.0902(23)	0.0897 13	0.000(3)	4180.00(4)	(3 <sup>-</sup> )	0.0170(10)	0.0172 9	0.000(2)
2290.57(3)	3 <sup>-</sup>	0.0561(15)	0.0772 16	0.0211(22)	4212.88(13)	(2 <sup>-</sup> ,3 <sup>+</sup> )	0.0067(7)	0.0050 5	-0.0016(9)
2397.14(4)	4 <sup>-</sup>	0.0256(15)	0.0253 10	0.000(2)	4250.8(4) <sup>c</sup>		0.0068(18)	0.0077 5	0.0009(19)
2419.111(23)	2 <sup>-</sup>	0.172(5)	0.201 3	0.029(6)	4253.91(4)	(2 <sup>-</sup> ) <sup>d</sup>	0.0840(20)	0.0922 25	0.008(3)
2575.92(4)	2 <sup>+</sup>	0.0427(17)	0.0622 14	0.0194(22)	4280.69(5)	2 <sup>-</sup>	0.0209(10)	0.023 4	0.002(4)
2625.91(3)	0 <sup>-</sup>	0.0547(18)	0.0575 12	0.0028(21)	4350.70(10)		0.0078(18)	0.0077 7	0.000(2)
2730.30(3)	1(1 <sup>-</sup> )	0.0486(19)	0.040 7	-0.009(7)	4396.15(7)	(0,1,2) <sup>-</sup>	0.0188(9)	0.0168 11	-0.0020(14)
2746.75(3)	(2,3) <sup>-</sup>	0.0058(4)	0.0131 9	0.0074(10)	4419.40(8)	(2 <sup>-</sup> ,3,4 <sup>+</sup> )	0.0044(6)	0.0058 6	0.0014(9)
2756.63(3)	2 <sup>+</sup>	0.0578(20)	0.0731 16	0.0153(25)	4463.61(8) <sup>c</sup>		0.0184(15)	0.0142 11	-0.0042(19)
2786.60(3)	3 <sup>+</sup>	0.0354(15)	0.0461 17	0.0106(22)	4473.19(6)	(2,3) <sup>-</sup>	0.0141(8)	0.0121 7	-0.0020(10)
2807.83(4)	(1,2) <sup>-</sup>	0.0556(18)	0.0628 17	0.0071(25)	4537.17(5)	2 <sup>-</sup>	0.0423(12)	0.0497 15	0.0074(19)
2986.06(4)	(2 <sup>-</sup> ,3 <sup>+</sup> )	0.0219(12)	0.019 6	-0.003(6)	4543.97(6) <sup>c</sup>		0.0066(6)	0.0075 8	0.0009(10)
3027.99(5)	2 <sup>-</sup>	0.0050(5)	0.0161 9	0.0111(10)	4662.30(24)	2 <sup>-</sup>	0.0048(5)	0.0050 6	0.0002(8)
3109.46(5)	(1,2) <sup>+</sup>	0.0108(8)	0.0114 8	0.0006(11)	4666.51(5) <sup>c</sup>		0.0075(6)	0.0077 10	0.000(2)
3128.45(5)	2 <sup>-</sup>	0.0263(13)	0.0289 11	0.0026(17)	4744.08(4)	(2 <sup>+</sup> )	0.0523(14)	0.052 3	0.000(3)
3146.39(5)	1	0.0161(10)	0.0276 10	0.0115(15)	4789.10(8)	(1 <sup>+</sup> )	0.0079(8)	0.0071 7	-0.0008(11)
3153.92(9)	(2,3) <sup>-</sup>	0.0034(5)	0.0075 11	0.0041(13)	4807.57(10)	(0 to 3) <sup>-</sup>	0.0073(8)	0.0111 7	0.0038(11)
3228.69(5)	2 <sup>-</sup>	0.0045(4)	0.0138 13	0.0093(13)	4850.35(7)		0.0099(7)	0.0125 10	0.0026(12)
3368.13(7)	(2,3) <sup>-</sup>	0.0129(10)	0.0151 16	0.0022(19)	4872.65(7)	(2,3) <sup>-</sup>	0.0116(8)	0.0108 7	-0.0008(11)
3393.65(7)	2 <sup>-</sup>	0.0118(10)	0.0133 8	0.0015(13)	4960.03(5) <sup>c</sup>	1 <sup>-</sup> ,2,3 <sup>+</sup>	0.0322(10)	0.0335 18	0.0013(20)
3414.34(4)	2 <sup>+</sup>	0.0312(12)	0.0302 11	-0.0010(16)	4993.07(5)	(2 <sup>-</sup> ,3 <sup>+</sup> )	0.0288(10)	0.0286 15	0.000(3)
3439.02(3)	(2 <sup>+</sup> )	0.0938(24)	0.0897 15	-0.004(3)	5024.14(15)		0.0038(6)	0.0036 4	0.0002(7)
3485.95(5)	2 <sup>-</sup>	0.0140(9)	0.0120 10	-0.0020(13)	5063.49(7)	(2 <sup>-</sup> ,3 <sup>+</sup> )	0.0130(8)	0.0123 9	-0.0007(12)
3557.04(6)	(1 <sup>-</sup> to 4 <sup>+</sup> )	0.0241(14)	0.0220 10	-0.0021(17)	5111.1(4)	2 <sup>-</sup>	0.0019(5)	0.0019 5	0.0000(7)
3599.35(4)	2 <sup>-</sup>	0.0464(16)	0.0471 15	0.000(2)	5189.57(6) <sup>c</sup>	2 <sup>-</sup> ,3 <sup>-</sup>	0.0213(7)	0.0198 13	-0.0015(14)
3629.97(7)	2 <sup>-</sup> ,3 <sup>-</sup>	0.0134(8)	0.0143 10	0.0009(13)	5213.56(11)	2 <sup>-</sup>	0.0022(3)	0.0046 5	0.0024(6)
3663.86(3)	(3,4) <sup>+</sup>	0.0634(19)	0.0625 14	-0.0009(24)	5246.86(16) <sup>c</sup>		0.00047(10)	0.00047 10	0.0000(2)
3713.20(8) <sup>c</sup>	2 <sup>-</sup> ,3 <sup>-</sup>	0.0079(8)	0.0042 6	-0.0037(10)	5488.71(9) <sup>c</sup>	2 <sup>-</sup> ,3	0.0091(6)	0.0149 11	0.0058(13)
3738.34(5)	1 <sup>+</sup>	0.0275(11)	0.0255 13	-0.002(17)	6097.27(12) <sup>c</sup>	1 <sup>-</sup> ,2,3	0.0054(5)	0.0055 6	0.0001(8)
3768.56(14)	0 <sup>-</sup> to 3 <sup>-</sup>	0.0071(6)	0.0027 5	-0.0044(8)	7799.57(2)	1 <sup>+</sup> ,2 <sup>+</sup>		1.948 12	1.948(12)

<sup>a</sup>Difference between cross section populating and depopulating the level.

<sup>b</sup>Sum of the observed cross section feeding the 0.0- and 29.8299-keV levels.

<sup>c</sup>New level assigned in this work.  $J^\pi$  deduced from the level scheme.

<sup>d</sup> $J^\pi = 3^-$  was assigned in ENSDF [11]. See discussion in the text.



transitions populate levels with both  $J^\pi = 3^-$  and  $J^\pi = 0^-$ , suggesting that neither spin strongly dominates.

The critical energy  $E_{\text{crit}}$  was set to 2.82 MeV in  $^{40}\text{K}$ . The total experimental intensity of primary  $\gamma$ -ray transitions to levels below  $E_{\text{crit}}$  is about 41% of the GS feeding. The remaining 59% of decays is subject to simulations based on the statistical model. The fraction of transitions to the GS and first excited state that escapes detection is estimated to be between 0.8 and 2.2% from various combinations of models and applied intensity thresholds. Assuming that less than 50 mb populates the ground state from subthreshold  $\gamma$  rays and no more than 6 mb populates it from unplaced  $\gamma$  rays the adopted cross section  $\sigma_0 = 2.28 \pm 0.04$  b.

The total experimental cross section feeding the GS and 29.8-keV state from levels below  $E_{\text{crit}} = 2.82$  MeV is  $1.836 \pm 0.014$  b. The simulated continuum feeding of the  $0 + 29.8$ -keV states from levels above  $E_{\text{crit}}$  is  $22 \pm 5\%$  giving a total cross section of  $2.35 \pm 0.15$  barns. The cross sections from both adopted approaches are completely consistent and agree with less precise previous measurements;  $3.0 \pm 1.5$  b [30],  $1.9 \pm 0.2$  b [31], and  $1.4$  b [32]. Mughabghab [29] adopted the cross section  $2.1 \pm 0.2$  b based partly on the EGAF [3] data.

Two 2787-keV levels were placed in ENSDF [11] with  $J^\pi = 3^+$  and  $3^-$ , respectively, with similar decay patterns. We only see  $\gamma$  rays previously assigned to the decay of the  $3^+$  state although the simulation strongly favors a negative parity assignment, which is also consistent with a strong primary  $\gamma$ -ray transition feeding this level. We propose that there is only one 2787-keV level with  $J^\pi = 3^-$  and that the second level reported at that energy may not exist.

The 2610.00-keV  $\gamma$ -ray placed deexciting the 4253.91-keV level has been reassigned as a primary transition deexciting the capture state to the 5189.57-keV level on the basis of intensity balance and energy. The 4253.91-keV level was originally assigned as  $J^\pi = 3^-$  [11] on the basis of  $L(d, p) = 1$ , unfavored parity in (pol  $d, \alpha$ ), and the 2610.00-keV  $\gamma$ -ray feeding the 1643.608-keV  $J^\pi = 0^+$  level. Reassigning the 2610.00-keV transition allows  $J^\pi = 2^-, 3^-$  for the 4253.91-keV level. The intense 2184.41-keV transition deexciting this level to the 2069.752-keV,  $J^\pi = 1^-$  level is unlikely to have  $E2$  multipolarity so the most likely spin assignment for the 4253.91-keV level is  $J^\pi = (2^-)$ .

Eighteen new levels at 3713.20-, 3797.58-, 4850.69-, 4350.70-, 4463.61-, 4543.97-, 4662.30-, 4666.51-, 4807.57-, 4850.35-, 4960.03-, 5024.14-, 5111.1-, 5189.57-, 5213.56-, 5246.86-, 5488.71-, and 6097-27 keV have been assigned to  $^{40}\text{K}$  in this work on the basis of energy sums, the presence of similar energy levels observed in reaction measurements, and the observation of a primary  $\gamma$  ray feeding the level.

The P-D diagram for  $^{40}\text{K}$  is shown in Fig. 2 where a good fit is obtained to nearly all levels below  $E_{\text{crit}}$ . There are only three levels that do not fit the P-D balance, levels at 2069.81 ( $3^-$ ), 2290.489 ( $3^-$ ), and 2746.91 ( $4^-$ ). All of them are too strongly populated in the experiment, compared to the simulation. Too strong (or weak) depopulation might be due to the misplaced (or missing) transitions. But we believe that this does not happen in this well-studied nucleus, at least for strong transitions.

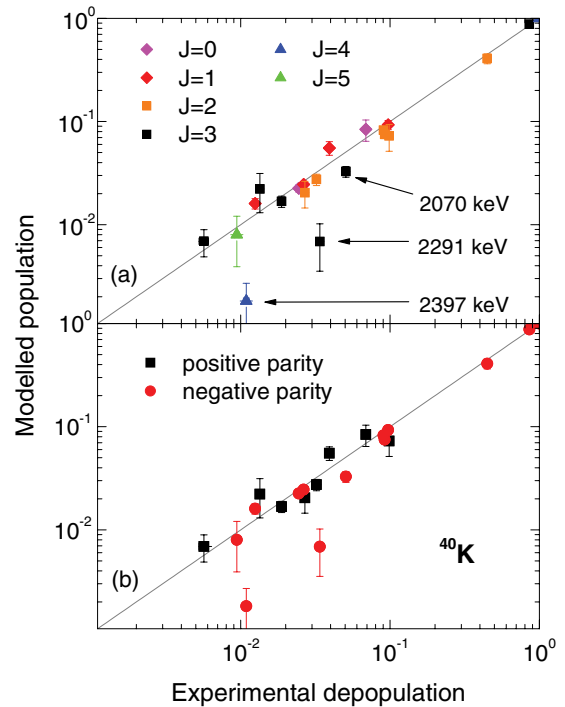


FIG. 2. (Color online) Population-depopulation plot for  $^{40}\text{K}$  colored by (a) spin and (b) parity (b). Simulations were made with models: SLO for  $E1$ , SP for  $M1$ , and BSGF for level density.

A reasonable agreement between simulated population and experimental depopulation of the 2069.81-keV level might be obtained only if  $J^\pi = 2^-$  is assumed for this level, although this would be inconsistent with the observed decay to the  $J^\pi = 5^-$  level and the experimentally observed  $M1(+E2)$   $\gamma$  ray to the  $J^\pi = 4^-$  ground state. A detailed inspection of the level scheme shows that the main source of strong feeding to the 2069.81-keV level is from the 4253.91-keV level. This level is unusually strongly populated by a primary  $\gamma$ -ray transition. The strong intensity of this primary transition is very likely due to direct neutron capture, consistent with the large observed spectroscopic factor in  $S(d, p)$  [11] that is typically proportional to the intensity of the primary transitions [29]. Such a strong primary transition, and subsequent feeding of the 2069.81-keV level thus cannot be explained within statistical model simulations. There is no primary transition feeding the 2290.489-keV level, which is populated only by levels other than the CS, and we are unable to find reasonable consistency with simulated feeding for any plausible spin/parity assignment ( $J^\pi = 3^-, 4^-$ ). We have no explanation for this discrepancy except to admit that the feeding of this level may not be adequately described by a statistical model.

A similar situation also occurs for the level at 2397.165 keV, assigned  $J^\pi = 4^-$  in ENSDF, which becomes consistent with the P-D diagram only if the spin is changed to  $3^+$ . This spin assignment is consistent with spins of levels whose  $\gamma$  rays populate/depopulate this level but inconsistent with  $L = 0$  for ( $d, ^3\text{He}$ ) and (pol  $d, \alpha$ ) reactions summarized in ENSDF [11] populating the level. The ( $d, ^3\text{He}$ ) measurement does not completely rule out a  $3^-$  assignment, which is also inconsistent with statistical model calculation.

TABLE IV.  $^{40,41}\text{K}(n, \gamma)$  thermal neutron capture  $\gamma$ -ray energies and cross sections measured in this work.  $I_\gamma$  and level assignments are from Krusche *et al.* [13,14].

$E_\gamma$ (keV)	$\sigma_\gamma$ (b)	$I_\gamma$ (relative)	Placement (initial→final)	$E_\gamma$ (keV)	$\sigma_\gamma$ (b)	$I_\gamma$ (relative)	Placement (initial→final)
$^{41}\text{K}$ transitions				$^{42}\text{K}$ transitions, continued			
981.14(19)	<20 <sup>a</sup>	3.44(74)	980 → 0	841.98(5)	0.197(7)	13.2(20)	842 → 0
1023.44(7)	<40 <sup>a</sup>	11.2(25)	2317 → 1294	938.92(16) <sup>b</sup>	0.030(4)	1.15(17)	1198 → 258
1293.82(11)	37.1(19)	40.5(86)	1294 → 0	1001.01(16) <sup>b</sup>	0.023(3)	1.49(22)	1843 → 842
1677.5(3)	13(3)	19.7(20)	1677 → 0	1110.49(16) <sup>b</sup>	0.028(4)	2.04(31)	1111 → 0
1697.20(25)	<21 <sup>a</sup>	8.13(81)	1698 → 0	1121.63(19) <sup>c</sup>	0.0308(4)	0.244(7)	2939 → 1817
$^{42}\text{K}$ transitions				1179.9(4)	0.027(8)	1.64(25)	1862 → 682
106.818(11)	0.499(10) <sup>a</sup>	32.9(66) <sup>a</sup>	107 → 0	1265.52(10) <sup>b</sup>	0.072(7)	3.73(56)	1266 → 0
151.64(3)	0.137(3)	10.7(22)	258 → 107	1377.22(17) <sup>b</sup>	0.031(4)	3.07(46)	1377 → 0
268.93(8)	0.035(3)	2.04(31)	1111 → 842	1408.22(19)	0.033(10)	2.99(45)	1408 → 0
376.96(19) <sup>b</sup>	0.012(3)	0.61(14)	1111 → 784	1862.05(17)	0.042(7)	3.43(51)	1862 → 0
380.52(8)	0.038(3)	2.50(50)	639 → 258	1937.0(3)	0.030(7)	1.50(23)	1937 → 0
431.69(6)	0.038(3)	2.89(58)	1274 → 842	2295.20(23)	0.073(8)	3.07(31)	2402 → 107
440.96(13) <sup>b</sup>	0.016(3)	1.26(25)	699 → 258	4768.6(4)	0.076(9)	4.11(21)	CS → 2766
444.92(14)	0.0126(25)	0.92(19)	1144 → 699	5131.8(4)	0.050(8)	3.69(18)	CS → 2402
453.84(21) <sup>c</sup>	0.0095(25)	0.275(56)	1862 → 1408	5167.9(4)	0.106(8)	6.56(33)	CS → 2366
504.88(9) <sup>b</sup>	0.031(4)	2.43(36)	1144 → 639	5295.8(3)	0.048(10)	2.65(31)	CS → 2239
531.95(5)	0.063(4)	5.52(86)	639 → 107	5460.6(4)	0.056(10)	2.52(13)	CS → 2072
595.93(21)	0.014(4)	0.83(12)	1862 → 1266	5671.9(4)	0.047(10)	3.71(19)	CS → 1862
616.31(14) <sup>b</sup>	0.030(4)	2.32(35)	1255 → 639	6156.3(5)	0.017(4)	0.901(45)	CS → 1377
621.08(15)	0.027(4)	1.34(20)	1464 → 842	6278.6(6)	0.019(4)	1.536(77)	CS → 1255
638.62(12)	0.047(7)	3.37(51)	639 → 0	6851.83(23)	0.080(7)	5.63(28)	CS → 682
681.96(3)	0.233(8)	15.5(23)	682 → 0	6894.0(5)	0.019(10)	1.252(63)	CS → 639
735.34(13)	0.044(4)	2.13(32)	842 → 107	7427.2(5)	0.027(7)	3.21(16)	CS → 107
783.79(10) <sup>b</sup>	0.037(4)	2.75(41)	784 → 0	7534.7(5)	0.030(7)	1.857(93)	CS → 0
831.57(22)	0.017(3)	0.052(9)	1513 → 682				

<sup>a</sup>Doublet with  $\gamma$  ray from  $^{40}\text{K}$ .<sup>b</sup>Transition of similar energy assigned to  $^{40}\text{K}$  [12].<sup>c</sup>Doublet placed in  $^{40}\text{K}$  and  $^{42}\text{K}$ .

The simulated population of the 2746.91-keV level, suggested as  $J^\pi = (2^-, 3^-)$  in ENSDF [11], is more consistent with a  $2^-$  spin assignment as shown in Fig. 2 although a good fit is also obtained for a  $3+$  spin assignment, which is also consistent with no strong primary transition feeding this level.

The spin and parity assignments in Table III were taken from ENSDF [11], except as indicated, and further limited by the assumption that all secondary  $\gamma$ -ray transitions have  $M1$ ,  $E1$ , or  $E2$  multipolarities and all primary transitions are  $M1$  or  $E1$ .

### B. $^{40}\text{K}(n, \gamma)^{41}\text{K}$

Table IV lists five  $\gamma$  rays that were assigned to  $^{41}\text{K}$  in this work. Three of these transitions are partly obscured by contaminants from  $^{40}\text{K}$ . The extensive  $^{41}\text{K}$  neutron capture  $\gamma$ -ray relative intensity data from Krusche *et al.* [13] can be renormalized using the 1293.586-keV ( $\sigma_\gamma = 37.1 \pm 1.9$  b) and 1677.198-keV ( $\sigma_\gamma = 13 \pm 3$  b)  $\gamma$ -ray cross sections measured in these experiments shown in Table V. These two  $\gamma$  rays account for about 50% of the total cross section feeding the GS of  $^{41}\text{K}$ . The weighted average normalization factor from both transitions is  $0.77 \pm 0.13$  for the Krusche *et al.* data and the total cross section observed feeding the GS of  $^{41}\text{K}$  is  $86 \pm 7$  b. The total energy weighted cross section is  $\Sigma E_\gamma \times I_\gamma = 73 \pm 7$  b for  $\gamma$  rays placed in the level scheme and  $6 \pm 2$  b for unplaced transitions. The  $^{41}\text{K}$  level scheme is well studied by

various reactions up to greater than 4 MeV and  $\gamma$  rays above 4 MeV that might populate the GS account for only 4 b.

The fraction of transition intensity to the GS escaping detection is estimated to be between 1.5 and 3.9% in the simulations. Assuming that less than 3 b populates the ground state from subthreshold  $\gamma$  rays and less than 4 b populates it from unplaced  $\gamma$  rays the deduced cross section is  $\sigma_0 = 90 \pm 8$  b. The total experimental cross section feeding the GS from levels below  $E_{\text{crit}} = 2.60$  MeV is  $75 \pm 4$  b. The simulated continuum feeding of the GS from levels above  $E_{\text{crit}}$  is about  $17 \pm 5\%$  giving a total cross section of  $90 \pm 7$  barns. These two values are again in excellent agreement. They are substantially higher than  $30 \pm 8$  barns measured by Beckstrand and Shera [33] and adopted by Mughabghab [29] but comparable to  $66 \pm 30$  barns measured by Pomerance [31] and  $\approx 70$  barns measured by Gillette [32].

The spin and parity of the GS of  $^{40}\text{K}$  is  $4^-$  so the capture state can be composed of  $J^\pi = 7/2^-$  and  $9/2^-$  resonances. Primary  $\gamma$  rays are observed to populate levels with  $J = 5/2$  but not  $J = 11/2$ , suggesting that the capture state is predominantly  $J^\pi = 7/2^-$ . This is confirmed by the DICEBOX simulations, which match the population of low- and high-spin states only if lower spin is responsible for 60–90% of all captures. The exact allowed range depends on the used PSF models. Only about 14% of the primary  $\gamma$ -ray intensity feeds the GS from levels below  $E_{\text{crit}} = 2.60$  MeV so a significant part of the decay scheme was simulated.

TABLE V. Cross sections populating and depopulating levels in  $^{41}\text{K}$  from the  $(n, \gamma)$  reaction. Level energies and  $J^\pi$  values are from the ENSDF [34].

Level energy (keV)	$J^\pi$	In <sup>a</sup> (b)	Out <sup>a</sup> (b)	Net <sup>b</sup> (b)	Level energy (keV)	$J^\pi$	In <sup>a</sup> (b)	Out <sup>a</sup> (b)	Net <sup>b</sup> (b)
0	$3/2^+$	95(5)		95(5)	4164.57(4)	$(5/2^+, 7/2, 9/2^+)$	1.25(6)	1.91(18)	-0.7(2)
980.476(8)	$1/2^+$	3.4(3)	3.2(6)	0.2(7)	4220.62(5)	$(5/2)$	0.96(6)	1.17(6)	-0.21(8)
1293.609(8)	$7/2^-$	41(3)	37.1(18)	4(3)	4228.99(5)	$(5/2)^-$	1.40(10)	1.86(10)	-0.5(1)
1559.903(12)	$3/2^+$	4.9(3)	4.6(4)	0.3(5)	4244.22(5)	$(3/2)^-$	1.99(9)	2.05(16)	-0.06(18)
1582.001(11)	$3/2^-$	4.05(19)	4.1(3)	-0.0(4)	4260.36(13)	$(3/2^-, 5/2)$	1.29(7)	1.10(7)	0.19(10)
1593.107(12)	$1/2^+$	0.60(3)	0.52(8)	0.08(8)	4274.96(5)	$(7/2^-, 9/2^+)$	2.77(13)	2.83(23)	-0.1(3)
1677.235(11)	$7/2^+$	17.3(10)	18.2(18)	-0.9(21)	4303.01(5)	$(5/2^+, 7/2^+)$	0.73(6)	0.71(5)	0.02(7)
1698.005(15)	$5/2^+$	5.3(3)	7.5(7)	-2.2(8)	4345.66(5)	$(5/2, 7/2^-)$	3.80(21)	3.37(21)	0.4(3)
2143.82(2)	$5/2^+$	4.46(19)	5.8(5)	-1.4(5)	4459.72(5)	$(3/2)^-$	1.63(7)	1.56(8)	0.07(11)
2166.70(2)	$3/2^-$	1.43(11)	1.26(16)	0.17(19)	4525.37(5)	$(3/2^-, 5/2, 7/2)$	0.27(4)	0.162(24)	0.11(4)
2316.62(2)	$5/2^-$	12.2(6)	11.1(23)	1.1(24)	4568.75(5)	$(9/2^+, 11/2^-)$	0.338(21)	0.55(3)	-0.21(4)
2447.83(7)	$3/2^+{}^c$	0.57(6)	0.42(4)	0.15(7)	4609.48(7)	$(5/2^+, 7/2, 9/2^+)$	1.64(7)	1.24(9)	0.4(1)
2494.91(3)	$9/2^+$	3.76(18)	4.3(5)	-0.5(6)	4730.70(5)	$(3/2)^-$	0.86(5)	0.53(3)	0.3(1)
2507.93(3)	$7/2^+$	4.37(23)	6.6(6)	-2.2(7)	4735.86(6)	$(5/2^+, 7/2^+)$	1.08(7)	1.41(8)	-0.3(1)
2527.66(3)	$11/2^+$	2.53(12)	2.8(6)	-0.3(6)	4745.49(10)	$(5/2^+)$	1.61(8)	1.71(6)	-0.1(1)
2593.97(3)	$1/2^-, 3/2^-$	0.51(3)	0.40(7)	0.11(7)	4749.47(8)	$(3/2^-, 5/2, 7/2^+)$	1.10(7)	1.25(5)	-0.2(1)
2710.3(3)	$3/2^+, 5/2^+$		0.252(25)	-0.25(3)	4823.33(5)	$(7/2^+, 9/2^+)$	2.11(11)	1.55(9)	0.6(1)
2712.57(3)	$(7/2^-)$	4.34(15)	4.4(7)	-0.1(7)	4862.43(6)	$(5/2)$	0.33(3)	0.45(3)	-0.12(4)
2756.73(3)	$5/2^+$	3.47(13)	4.3(4)	-0.8(4)	4927.83(6)	$(5/2)^+$	1.18(5)	1.77(19)	-0.6(2)
2761.73(3)	$11/2^-$	1.67(12)	3.0(6)	-1.3(6)	4948.94(6)	$(3/2^-, 5/2, 7/2^-)$	0.35(3)	0.52(3)	-0.17(4)
2774.25(3)	$13/2^+$	0.52(4)	0.49(7)	0.03(8)	5021.23(8)	$(5/2^+)$	0.229(22)	0.213(19)	0.02(3)
3048.22(5)	$1/2^-, 3/2^-$	0.67(3)	0.49(4)	0.18(5)	5096.20(8)	$(5/2, 7/2, 9/2^-)$	0.81(4)	0.52(5)	0.3(1)
3141.84(3)	$(7/2^-)$	0.76(6)	1.16(18)	-0.40(19)	5185.27(6)	$(5/2, 7/2^-)$	0.91(6)	0.63(4)	0.3(1)
3142.43(3)	$5/2^-$	3.28(15)	4.5(4)	-1.2(5)	5298.86(6)	$(3/2^-, 5/2, 7/2^-)$	1.07(9)	0.81(7)	0.26(11)
3213.61(4)	$5/2^-$	1.63(8)	2.23(20)	-0.6(2)	5496.61(7)	$(7/2^+)$	0.96(6)	1.49(8)	-0.5(1)
3235.57(4)	$(3/2^-, 5/2, 7/2)$	1.51(16)	2.53(25)	-1.0(3)	5548.19(7)	$(5/2^+, 7/2^+)$	1.15(6)	1.15(5)	0.00(7)
3240.65(4)	$(5/2^+, 7/2^-)$	1.680(8)	1.80(16)	-0.12(18)	5557.39(9)	$(3/2^-, 5/2^+)$	0.24(4)	0.329(18)	-0.09(4)
3431.84(4)	$(9/2^-, 7/2^-)$	1.41(12)	1.72(15)	-0.3(2)	5575.24(8)	$(3/2^-, 5/2, 7/2^+)$	0.43(3)	0.60(4)	-0.17(5)
3450.1(2)	$5/2^-, 7/2^-$		1.16(12)	-1.2(1)	5604.58(8)	$(3/2^-, 5/2, 7/2^+)$	0.355(21)	0.44(3)	-0.09(4)
3488.5(3)	$(5/2)^+$	0.132(15)	0.063(7)	0.07(2)	5610.83(6)	$(5/2, 7/2^+)$	0.319(18)	0.230(25)	0.09(3)
3489.41(7)	$(5/2, 7/2)^-$	0.137(25)	0.33(3)	-0.19(4)	5655.66(8)	$(3/2^-, 5/2^+)$	1.25(6)	1.55(11)	-0.3(1)
3521.38(9)	$(5/2^+, 7/2^+)$	0.402(20)	0.51(4)	-0.10(4)	5659.25(8)	$(3/2^-, 5/2, 7/2^+)$	0.50(3)	0.358(22)	0.14(4)
3534.45(4)	$(7/2^+, 9/2)$	0.68(4)	1.06(15)	-0.38(15)	5800.80(7)	$(3/2^+, 5/2^+)$	0.50(3)	0.80(6)	-0.3(1)
3560.61(5)	$(3/2^-, 5/2, 7/2^+)$	0.52(3)	0.42(11)	0.1(1)	5826.66(7)	$(5/2)^+$	0.82(5)	0.88(6)	-0.06(8)
3572.38(5)	$(3/2^+, 5/2, 7/2^-)$		1.18(13)	-1.2(1)	5886.95(8)	$(3/2)^-$	0.74(3)	0.62(6)	0.12(7)
3612.77(5)	$(3/2^-, 5/2^+)$	0.54(4)	0.340(19)	0.17(4)	5912.50(8)	$(9/2^+)$	0.79(4)	1.45(6)	-0.7(1)
3651.46(5)	$(5/2, 7/2, 9/2^+)$	0.89(5)	1.21(11)	0.32(13)	5952.41(8)	$(7/2^-, 9/2, 11/2^-)$	0.64(3)	0.39(3)	0.25(5)
3761.54(5)	$(5/2^+, 7/2^+)$	2.09(11)	2.00(9)	0.09(14)	5968.89(8)	$(9/2^+, 11/2^-)$	0.359(19)	0.32(4)	0.03(4)
3774.66(5)	$5/2^-, 7/2^-$	1.35(6)	1.78(10)	-0.4(1)	6040.67(10)	$(3/2^-, 5/2, 7/2)$	0.68(4)	0.72(5)	-0.04(7)
3826.90(10)	$(5/2, 7/2^+)$	1.09(5)	0.95(6)	0.14(7)	6070.76(9)	$(5/2, 7/2, 9/2^+)$	0.45(3)	0.50(4)	-0.05(5)
3870.52(6)	$5/2^-, 7/2^-$	0.28(4)	0.210(18)	0.07(5)	6078.56(7)	$(3/2)^-$	0.52(3)	0.41(34)	0.11(4)
3990.40(5)	$(7/2^- 9/2, 11/2^+)$	0.54(4)	0.30(5)	0.24(6)	6186.04(11)	$(5/2, 7/2)$	1.43(7)	1.54(8)	-0.1(1)
3996.49(4)	$(5/2^+)$	5.9(3)	6.22(23)	-0.3(4)	6211.50(7)	$(7/2^+, 9/2^-)$	1.06(5)	0.99(4)	0.07(7)
4026.94(7)	$(3/2^-, 5/2, 7/2^+)$	0.90(6)	0.66(6)	0.24(8)	6229.88(10)	$(3/2^-, 5/2, 7/2^-)$	0.299(19)	0.45(4)	-0.15(5)
4146.15(6)	$5/2^-, 7/2^-$	1.08(5)	0.80(8)	0.28(9)	6255.96(8)	$(5/2, 7/2^-)$	0.53(3)	0.55(3)	-0.02(4)
6290.05(14)	$(3/2)^-$	0.89(5)	0.76(3)	0.13(6)	7020.97(10)	$(3/2)^-$	1.06(6)	1.13(7)	-0.07(9)
6394.31(10)	$(3/2^-, 5/2, 7/2^-)$	0.48(3)	0.75(4)	-0.27(5)	7035.28(14)	$(5/2)^-$	0.80(5)	0.98(5)	-0.18(7)
6434.51(9)	$(3/2^-, 5/2, 7/2^-)$	0.59(4)	0.80(4)	-0.21(5)	7361.15(11)	$(3/2^-, 5/2, 7/2^-)$	0.50(5)	0.74(5)	-0.24(7)
6450.15(10)	$(3/2^-, 5/2, 7/2^+)$	0.213(24)	0.53(4)	-0.32(4)	7593.06(9)	$(5/2^+ \text{ to } 11/2^-)$	0.67(6)	0.57(6)	0.1(1)
6497.00(10)	$(3/2)^-$	0.214(16)	0.123(15)	0.09(2)	7654.93(9)	$(3/2^-, 5/2, 7/2^-)$	0.79(8)	1.45(5)	-0.7(1)
6528.13(9)	$(3/2^-, 5/2, 7/2^-)$	0.69(12)	1.13(6)	-0.4(1)	7938.98(10)	$(5/2 \text{ to } 11/2^-)$	1.16(12)	0.82(4)	0.3(1)
6769.77(10)	$(3/2^-, 5/2, 7/2^-)$	0.45(3)	0.54(7)	-0.09(8)	8190.21(12)	$(3/2^-, 5/2, 7/2^-)$	0.29(3)	0.56(4)	-0.27(5)
6782.54(10)	$3/2^- \text{ to } 9/2^-$	0.46(3)	0.41(5)	-0.05(6)	8200.11(9)	$(3/2^-, 5/2, 7/2^-)$	1.027(11)	1.29(6)	-0.3(1)
6791.36(9)	$(5/2, 7/2, 9/2^-)$	0.35(3)	0.50(3)	-0.15(4)	9740.70(10)	$(3/2)^-$	0.103(16)	0.093(12)	0.01(2)
6835.43(9)	$(5/2, 7/2^-)$	0.99(7)	1.14(5)	-0.15(9)	10095.243(15) <sup>d</sup>	$7/2^-, 9/2^-$		80.3(8)	-80.3(8)
6995.53(11)	$(5/2, 7/2, 9/2^+)$	0.378(25)	0.56(3)	-0.18(4)					

<sup>a</sup>Includes the intensity of multiply placed transitions.<sup>b</sup>Difference between cross-section populating and depopulating levels.<sup>c</sup>See text for a discussion of spin assignment.<sup>d</sup> $S_n$  from a least squared fit of the primary  $\gamma$ -ray energies from reference [13] to the adopted level energies from Evaluated Nuclear Structure Data File [34].

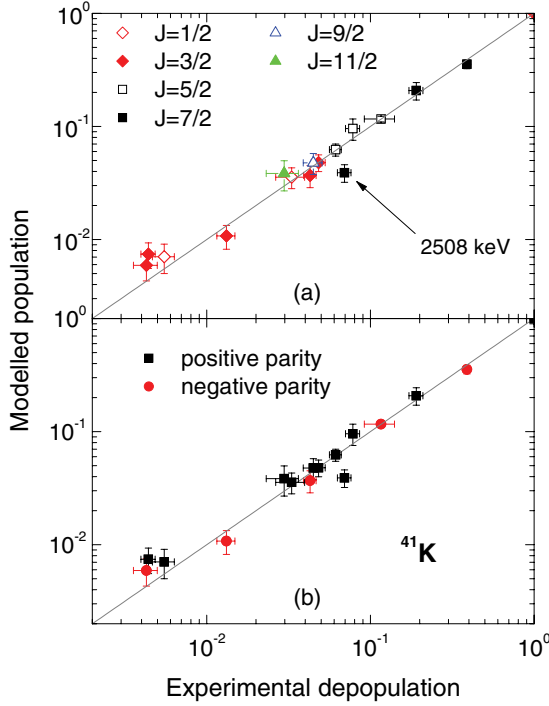


FIG. 3. (Color online) Population-depopulation plot for  $^{41}\text{K}$  colored by (a) spin and (b) parity. Simulations were made with models: SLO for  $E1$ , SP for  $M1$ , and BSGF for level density.

The P-D plot for levels in  $^{41}\text{K}$  is shown in Fig. 3. Very good agreement is achieved between the population and depopulation of all but one level below  $E_{\text{crit}}$ . The  $J^\pi = 7/2^+$  level at 2507.93 keV [34] has significantly higher experimental depopulation than simulated population. In this case the  $J^\pi$  assignment is based on the level's  $\gamma$ -ray deexcitation pattern and the parity measured by  $\gamma(\theta, \text{pol})$  in  $(\alpha, p\gamma)$  [35].  $J^\pi = 5/2^-$  can bring the experiment and simulation into reasonable agreement, which is consistent with the decay of this level but is inconsistent with  $E2$  character assigned to  $\gamma$  rays deexciting it to  $J^\pi = (3/2^+)$  levels. The level at 2447.83-keV was assigned  $(3/2^+, 5/2, 7/2^+)$  in ENSDF [34], but reasonable agreement between the simulated population and the experimental depopulation is only achieved for  $J^\pi = 3/2^+$ . This is consistent with  $\ell_p = (0, 2)$  for  $^{42}\text{Ca}(t, \alpha)$  [36]. The simulated populations for  $J^\pi = 5/2^+$  and  $J^\pi = 7/2^+$  assignments to this level are too large.

### C. $^{41}\text{K}(n, \gamma)^{42}\text{K}$

Table IV lists 43  $\gamma$  rays assigned to  $^{42}\text{K}$  that were measured in this work. These transitions were assigned to  $^{42}\text{K}$  by comparison with the more extensive  $\gamma$ -ray intensities measured by Krusche *et al.* [14]. Several  $\gamma$  rays assigned to  $^{42}\text{K}$  have similar energies to the transitions assigned to  $^{40}\text{K}$  [12]. We used a planar, low-energy photon spectrometer (LEPS) to carefully inspect the first excited state energy region at 107 keV for possible interference from transitions in  $^{40}\text{K}$  near that energy. One 0.54-mb transition was found which was too weak to affect this analysis. A least-squares fit to the Budapest  $\sigma_\gamma$  data and Krusche *et al.* intensity

data gave a normalization factor of  $N = 0.0154 \pm 0.0003$  for converting the relative  $\gamma$ -ray intensity data to the cross-section scale. The cross sections populating and depopulating levels in  $^{42}\text{K}$  from the combined measurements are shown in Table VI where the total cross section observed feeding the GS of  $^{42}\text{K}$  is  $1.604 \pm 0.023$  b. The total energy weighted cross section is  $\Sigma E_\gamma \times I_\gamma = 1.48 \pm 0.03$  b for  $\gamma$  rays placed in the level scheme and  $0.06 \pm 0.01$  b for unplaced transitions. The  $^{42}\text{K}$  level scheme is well studied by various reactions up to approximately 4 MeV and unplaced  $\gamma$  rays with energies  $>4$  MeV that could feed the GS have a total cross section of less than 14 mb.

The intensity of the primary transitions feeding levels below  $E_{\text{crit}} = 1.4$  MeV is about 18% of the total GS feeding and the remaining decay scheme intensity has been simulated. The GS of  $^{41}\text{K}$  is  $3/2^+$  so the capture state can be composed of  $J^\pi = 1^+$  and  $2^+$  resonances. The primary  $\gamma$  rays are observed to levels with  $J^\pi = 3^-$ , indicating that higher spin must significantly contribute to capturing state, but the absence of known levels with  $J = 0$  and 1 at low excitations in  $^{42}\text{K}$  makes the calculation insensitive to the contribution of the lower spin resonances.

The simulated fraction of the transition intensity that escapes detection feeding to GS obtained from simulations with different model combinations is 0.4–1.4%. Assuming that less than 14 mb populates the ground state from subthreshold  $\gamma$  rays and less than 21 mb populates it from unplaced  $\gamma$  rays the deduced cross section is  $\sigma_0 = 1.62 \pm 0.03$  b. The total experimental cross section feeding the GS from levels below  $E_{\text{crit}} = 1.40$  MeV is  $1.185 \pm 0.019$  b. A simulated GS

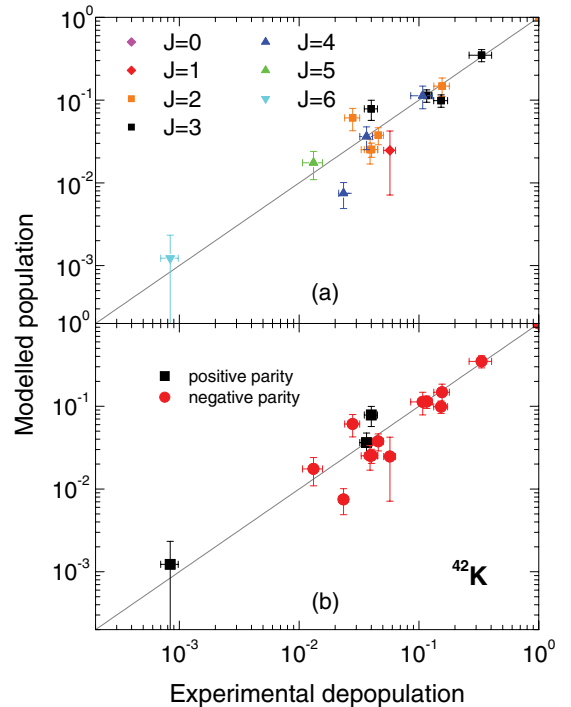


FIG. 4. (Color online) Population-depopulation plot for  $^{42}\text{K}$  colored by (a) spin and (b) parity. Simulations were made with models: SLO for  $E1$ , SP for  $M1$ , and BSGF for level density.



TABLE VI. Cross sections populating and depopulating levels in  $^{42}\text{K}$  from the  $(n, \gamma)$  reaction. Level energies and  $J^\pi$  values are from the ENSDF [37].

Level energy (keV)	$J^\pi$	In <sup>a</sup> (b)	Out <sup>a</sup> (b)	Net <sup>b</sup> (b)	Level energy (keV)	$J^\pi$	In <sup>a</sup> (b)	Out <sup>a</sup> (b)	Net <sup>b</sup> (b)
0	2 <sup>-</sup>	1.604(23)		1.604(23)	2607.02(6)	(1 <sup>-</sup> ,2,3)	0.0110(5)	0.0065(5)	0.0045(7)
106.828(7)	3 <sup>-</sup>	0.508(9)	0.504(10)	0.004(14)	2627.85(6)	(2 <sup>-</sup> ,3)	0.0140(6)	0.0151(10)	-0.001(1)
258.261(8)	4 <sup>-</sup>	0.151(6)	0.138(3)	0.014(7)	2644.31(6)	3 <sup>-</sup>	0.0144(7)	0.0135(13)	0.001(2)
638.726(12)	3 <sup>-</sup>	0.164(7)	0.148(9)	0.016(11)	2653.79(11)	(2 <sup>-</sup> ,3)	0.00095(6)	0.0041(3)	-0.0032(3)
681.943(11)	(2,3)	0.234(7)	0.235(8)	-0.001(10)	2718.12(6)	(2 <sup>-</sup> ,3)	0.0248(12)	0.0255(19)	-0.001(2)
699.08(3)	5 <sup>-</sup>	0.0198(25)	0.016(3)	0.004(4)	2765.96(6)	(2 <sup>+</sup> ,3)	0.068(3)	0.068(4)	-0.000(5)
783.87(20)	2 <sup>-</sup>	0.0448(20)	0.042(6)	0.003(6)	2862.71(7)	(2 <sup>-</sup> ,3)	0.0091(4)	0.0255(21)	-0.016(2)
841.940(12)	3 <sup>-</sup>	0.221(7)	0.237(8)	-0.016(10)	2877.98(6)	3 <sup>-</sup>	0.0102(4)	0.0109(6)	-0.0007(8)
1110.747(17)	3 <sup>+</sup>	0.0411(23)	0.070(5)	-0.029(6)	2917.02(8)	(1 <sup>-</sup> -4 <sup>+</sup> )	0.00493(24)	0.0040(4)	0.0010(4)
1143.59(1.9)	4 <sup>+</sup>	0.0418(22)	0.049(5)	-0.007(5)	2926.09(6)	(2,3) <sup>-</sup>	0.0097(4)	0.0074(6)	0.002(1)
1197.90(2)	4 <sup>-</sup>	0.0354(19)	0.036(3)	-0.006(4)	2938.59(7)	(1 <sup>-</sup> ,2,3)	0.0097(5)	0.0087(12)	0.001(1)
1254.820(19)	(2,3) <sup>-</sup>	0.068(3)	0.070(6)	-0.002(7)	3008.35(7)	3	0.0137(7)	0.0128(7)	0.001(1)
1266.305(18)	(1,2,3) <sup>-</sup>	0.075(3)	0.109(8)	-0.034(8)	3014.46(7)	(1 <sup>-</sup> -4 <sup>+</sup> )	0.0098(5)	0.0116(8)	-0.002(1)
1273.54(2)	(2 <sup>-</sup> ,3,4 <sup>+</sup> )	0.040(3)	0.053(3)	-0.013(4)	3021.10(7)	(2 <sup>-</sup> ,3)	0.0196(10)	0.0145(13)	0.005(1)
1375.96(10)	6 <sup>+</sup>	0.00027(3)	0.00116(20)	-0.0009(2)	3040.15(8)	3 <sup>-</sup>	0.0066(3)	0.0066(4)	0.0000(5)
1377.12(2)	(2,3) <sup>-</sup>	0.0474(16)	0.063(7)	-0.015(8)	3195.82(7)	(2 <sup>-</sup> ,3)	0.0126(6)	0.0128(7)	-0.0002(9)
1400.04(5)	(2,3)	0.0126(5)	0.0134(17)	-0.001(2)	3210.64(7)	(1 <sup>+</sup> ,2,3)	0.0070(3)	0.00470(25)	0.0023(4)
1407.922(19)	(1 <sup>-</sup> ,2,3)	0.059(4)	0.053(5)	0.006(6)	3233.92(7)	(3,4 <sup>+</sup> )	0.0121(7)	0.0095(6)	0.003(1)
1453.07(5)	(2 <sup>-</sup> ,3,4 <sup>-</sup> )	0.0081(5)	0.0061(15)	0.002(2)	3284.40(7)	(2,3) <sup>-</sup>	0.0146(7)	0.0197(12)	-0.005(1)
1463.65(2)	(1 <sup>-</sup> ,2,3)	0.0220(7)	0.0270(25)	-0.005(3)	3287.19(7)	(2 <sup>-</sup> ,3,4 <sup>+</sup> )	0.0042(3)	0.0102(5)	-0.006(1)
1489.29(9)	(1 <sup>-</sup> -5 <sup>-</sup> )	0.00195(17)	0.00054(12)	0.0014(2)	3295.32(9)	(2,3)	0.00404(19)	0.00199(16)	0.0020(3)
1513.08(4)	(1 <sup>-</sup> -5 <sup>-</sup> )	0.0042(3)	0.0053(7)	-0.0012(8)	3304.34(9)	(1 <sup>+</sup> -4 <sup>+</sup> )	0.00477(21)	0.0042(4)	0.0006(5)
1538.73(7)	(3,5) <sup>+</sup>	0.00210(24)	0.0021(4)	0.0000(5)	3323.74(8)	3 <sup>-</sup>	0.00343(20)	0.00491(25)	-0.0015(3)
1692.00(4)	(1 <sup>-</sup> -5 <sup>-</sup> )	0.00284(17)	0.0027(4)	0.0002(4)	3367.34(8)	(0 <sup>-</sup> -3 <sup>+</sup> )	0.0065(4)	0.0051(4)	0.0014(5)
1723.42(4)	(2,3,4 <sup>+</sup> )	0.0148(7)	0.0147(20)	0.000(2)	3418.45(8)	(2,3) <sup>-</sup>	0.0276(15)	0.02564(13)	0.002(2)
1745.61(3)	(2 <sup>+</sup> ,3,4 <sup>+</sup> )	0.0111(6)	0.0123(13)	-0.001(1)	3421.28(8)	(0 <sup>-</sup> -3 <sup>+</sup> )	0.0108(5)	0.0117(7)	-0.001(1)
1816.87(3)	(2,3)	0.0175(13)	0.0186(25)	-0.001(3)	3502.90(8)	(2 <sup>+</sup> ,3,4 <sup>+</sup> )	0.0073(4)	0.0092(6)	-0.002(1)
1842.98(3)	(1 <sup>-</sup> ,2,3)	0.0426(16)	0.049(4)	-0.007(4)	3528.95(17)	(0 <sup>-</sup> -3)	0.00159(10)	0.0043(4)	-0.0027(4)
1861.90(2)	2 <sup>-</sup>	0.092(4)	0.104(6)	-0.012(8)	3621.24(9)	(2,3)	0.0065(3)	0.0046(4)	0.002(1)
1913.48(2)	(2 <sup>-</sup> ,3)	0.0118(9)	0.0116(14)	0.000(2)	3658.59(8)	(2 <sup>-</sup> ,3)	0.0150(10)	0.0156(7)	-0.001(1)
1937.50(2)	(1,2,3) <sup>-</sup>	0.046(3)	0.061(5)	-0.015(6)	3674.15(8)	(1 <sup>-</sup> ,2,3)	0.0089(4)	0.0087(6)	0.0002(7)
1987.97(3)	(1 <sup>-</sup> -4 <sup>-</sup> )	0.0070(7)	0.0128(15)	-0.006(2)	3696.44(10)	(3 <sup>-</sup> ,4 <sup>+</sup> )	0.0147(7)	0.0115(4)	0.003(1)
2049.32(4)	3 <sup>+</sup>	0.0336(16)	0.031(3)	0.003(4)	3770.64(10)	(0 <sup>-</sup> -3)	0.00155(7)	0.00249(16)	-0.0009(2)
2072.00(4)	(2,3) <sup>-</sup>	0.0482(21)	0.059(4)	-0.011(4)	3794.64(9)	(0-3)	0.0117(6)	0.0111(8)	0.001(1)
2161.62(6)	(2 <sup>+</sup> ,3,4 <sup>+</sup> )	0.0097(5)	0.0098(11)	-0.000(2)	3798.15(10)	(2 <sup>-</sup> ,3,4 <sup>+</sup> )	0.00308(15)	0.00297(20)	0.0001(2)
2187.20(7)	3 <sup>+</sup>	0.00343(23)	0.0031(3)	0.0004(4)	3831.71(10)	(1 <sup>+</sup> ,2,3)	0.00179(10)	0.00198(16)	0.0002(2)
2204.03(6)	(2 <sup>-</sup> ,3,4 <sup>+</sup> )	0.0084(6)	0.0069(10)	0.0015(12)	3861.99(9)	(1 <sup>-</sup> -4 <sup>+</sup> )	0.0132(6)	0.0108(7)	0.002(1)
2238.62(5)	(1,2,3) <sup>-</sup>	0.0421(20)	0.047(4)	-0.005(4)	3876.98(8)	(1 <sup>-</sup> -4 <sup>+</sup> )	0.0111(5)	0.01357(5)	-0.002(1)
2251.09(5)	(0 <sup>-</sup> -4 <sup>-</sup> )	0.0133(7)	0.0127(20)	0.001(2)	3888.34(10)	(1 <sup>+</sup> -4 <sup>+</sup> )	0.00232(20)	0.0037(5)	-0.0014(5)
2366.19(5)	(2,3) <sup>-</sup>	0.108(4)	0.110(7)	-0.002(8)	3890.13(9)	(0 <sup>-</sup> -3)	0.0076(5)	0.0043(3)	0.003(1)
2388.83(6)	3 <sup>-</sup>	0.0185(8)	0.0226(18)	-0.004(2)	3934.64(10)	(2 <sup>-</sup> ,3,4 <sup>+</sup> )	0.00519(25)	0.0047(7)	0.0005(8)
2401.82(5)	(2,3) <sup>-</sup>	0.064(3)	0.091(4)	-0.027(5)	4013.92(9)	(1 <sup>+</sup> ,2,3)	0.0221(12)	0.0205(7)	0.002(1)
2422.13(5)	(1 <sup>-</sup> ,2,3)	0.0334(15)	0.0373(25)	-0.004(3)	4036.93(11)	3 <sup>-</sup>	0.0080(3)	0.0065(5)	0.002(1)
2482.16(5)	(1,2,3) <sup>-</sup>	0.0344(16)	0.025(3)	0.010(3)	4039.95(8)	(1 <sup>+</sup> ,2,3)	0.0047(3)	0.0057(5)	-0.001(1)
2573.63(6)	(2,3)	0.0076(4)	0.0079(8)	0.0003(8)	4053.90(9)	(1 <sup>+</sup> ,2,3)	0.00474(25)	0.0040(3)	0.0007(4)
4103.77(10)	(1 <sup>-</sup> -4 <sup>+</sup> )	0.0051(3)	0.0031(4)	0.0020(5)	4878.6(3)	(1 <sup>+</sup> -4 <sup>+</sup> )	0.00196(20)	0.0058(3)	-0.0039(4)
4105.3(4)	(0 <sup>-</sup> -3)	0.00353(20)	0.00383(21)	-0.0003(3)	4903.70(10)	(3 <sup>-</sup> ,4 <sup>+</sup> )	0.00191(20)	0.0036(3)	-0.0017(3)
4128.34(9)	(2 <sup>+</sup> ,3)	0.0317(15)	0.0311(10)	0.001(2)	4938.98(10)	(1 <sup>-</sup> ,2,3)	0.00196(25)	0.00398(19)	-0.0020(3)
4152.39(9)	(2 <sup>-</sup> ,3,4 <sup>+</sup> )	0.0100(5)	0.0094(3)	0.001(1)	4942.98(10)	(1 <sup>-</sup> -4 <sup>-</sup> )	0.0030(3)	0.0032(4)	-0.0002(5)
4154.67(11)	(1 <sup>-</sup> ,2,3)	0.00328(20)	0.00408(23)	-0.0008(3)	4959.65(10)	(0-4 <sup>+</sup> )	0.0018(6)	0.00165(8)	0.000(1)
4179.44(10)	(2 <sup>-</sup> ,3,4 <sup>+</sup> )	0.00252(15)	0.00152(16)	0.0010(2)	5003.00(10)	(1 <sup>-</sup> ,2,3)	0.0050(5)	0.0048(3)	0.0002(6)
4259.12(10)	(1 <sup>-</sup> ,2,3)	0.00183(11)	0.00356(18)	-0.0017(2)	5064.02(10)	(1 <sup>-</sup> -4 <sup>+</sup> )	0.0046(4)	0.00678(23)	-0.0022(5)
4389.78(15)	(2 <sup>-</sup> ,3,4 <sup>+</sup> )	0.00429(20)	0.00299(18)	0.0013(3)	5081.27(10)	(1 <sup>-</sup> ,2,3)	0.0035(4)	0.00287(13)	0.0006(4)
4416.61(9)	(2 <sup>-</sup> ,3)	0.0192(10)	0.0168(6)	0.002(1)	5097.05(10)	(0 <sup>-</sup> -3)	0.0050(5)	0.0051(3)	-0.0001(6)
4428.25(9)	(1 <sup>+</sup> ,2,3)	0.0131(6)	0.0121(6)	0.001(1)	5179.14(10)	(0 <sup>-</sup> -4 <sup>+</sup> )	0.00202(20)	0.00183(20)	0.0002(3)
4443.15(10)	(0 <sup>-</sup> -4 <sup>+</sup> )	0.00323(20)	0.0034(3)	-0.0002(4)	5246.64(10)	(1-4 <sup>+</sup> )	0.0070(7)	0.00380(18)	0.003(1)
4481.05(10)	(2,3)	0.0122(6)	0.0088(5)	0.003(1)	5318.96(10)	(2 <sup>-</sup> ,3)	0.0027(4)	0.00398(19)	-0.0013(4)
4556.67(10)	(1 <sup>-</sup> ,2,3)	0.0082(8)	0.0078(5)	0.0004(9)	5476.94(10)	(1 <sup>+</sup> ,2,3)	0.00096(15)	0.00089(7)	0.0001(2)
4576.26(10)	(2,3) <sup>-</sup>	0.0055(5)	0.0067(3)	-0.001(1)	5630.28(10)	(0-4 <sup>+</sup> )	0.00078(13)	0.00115(12)	-0.0004(2)
4590.59(10)	(2 <sup>-</sup> ,3,4 <sup>+</sup> )	0.0065(6)	0.0109(4)	-0.004(1)	5697.23(10)	(0-4 <sup>+</sup> )	0.0021(3)	0.00377(16)	-0.0017(3)
4612.78(11)	(2 <sup>+</sup> ,3)	0.0038(11)	0.0062(4)	-0.002(1)	5710.62(10)	(2 <sup>-</sup> ,3,4 <sup>+</sup> )	0.0051(7)	0.0034(3)	0.002(1)
4660.73(13)	(2 <sup>-</sup> ,3)	0.0040(4)	0.00299(19)	0.0010(4)	5759.70(10)	(0 <sup>-</sup> -4 <sup>+</sup> )	0.0024(3)	0.0042(3)	-0.0018(4)
4715.41(17)	(2 <sup>-</sup> ,3)	0.00151(15)	0.00182(15)	-0.0003(2)	5789.71(10)	(0-4 <sup>+</sup> )	0.0032(4)	0.0026(3)	0.0006(5)

TABLE VI. (Continued.)

Level energy (keV)	$J^\pi$	In <sup>a</sup> (b)	Out <sup>a</sup> (b)	Net <sup>b</sup> (b)	Level energy (keV)	$J^\pi$	In <sup>a</sup> (b)	Out <sup>a</sup> (b)	Net <sup>b</sup> (b)
4748.54(13)	$3^-$	0.00177(20)	0.0042(3)	-0.0025(3)	5846.59(10)	$(1^+4^+)$	0.00064(11)	0.00110(11)	0.0005(2)
4778.04(12)	$(1^-4^+)$	0.00237(25)	0.0043(3)	-0.0019(4)	5953.51(10)	$(1-4^+)$	0.0046(7)	0.0054(3)	-0.001(1)
4806.84(10)	$(0-3)^-$	0.0171(15)	0.0136(6)	0.004(2)	5978.36(10)	$(1-4^+)$	0.00182(25)	0.00382(23)	-0.0020(3)
4853.60(10)	$(0-3)^-$	0.0095(10)	0.0055(3)	0.004(1)	7533.829(10)	$1^+, 2^+$		1.434(10)	-1.434(10)

<sup>a</sup>Includes the intensity of multiply placed transitions.

<sup>b</sup>Difference between cross section populating and depopulating levels.

<sup>c</sup>Level placement from ENSDF [34].

<sup>d</sup> $S_n$  from a least-squared fit of the primary  $\gamma$ -ray energies from Ref. [13] to the adopted level energies from the ENSDF [37].

feeding from levels above  $E_{\text{crit}}$  is  $24 \pm 7\%$ , giving a total cross section for  $^{41}\text{K}$  of  $\sigma_0 = 1.56 \pm 0.15$  b. Again, the values of  $\sigma_0$  obtained with the two approaches are in excellent agreement. The resulting  $\sigma_0$  is higher than most previous results shown in Table VII and inconsistent with the value adopted by Mughabghab [29]  $\sigma_0 = 1.46 \pm 0.03$  b.

The P-D plot for levels in  $^{42}\text{K}$  using the ENSDF  $J^\pi$  assignments [37] is shown in Fig. 4. The agreement is nearly as good as for the other potassium isotopes despite the very low value of  $E_{\text{crit}}$  used in the simulations and problems with adopted level scheme at low excitation energies including the indefinite spin assignment for levels near 1.2 MeV. A significant improvement is possible by changing the spin or parity of several levels. These changes were found to have little effect on the deduced value of  $\sigma_0$ . A better fit is achieved with the  $J^\pi$  assignments proposed in the P-D plot shown in Fig. 5.

#### D. $^{41}\text{K}(n,\gamma)^{42}\text{K}$ activation measurement

The  $1524.66 \pm 0.08$ -keV  $\gamma$  ray from  $^{42}\text{K}$   $\beta^-$  decay,  $t_{1/2} = 12.321 \pm 0.025$  h [38], was observed in a low background chamber following the prompt  $\gamma$ -ray experiment after the neutron beam was turned off. Its cross section was determined as  $0.269 \pm 0.005$  b after correction for the production and decay during bombardment. This value is in good agreement with the four previous measurements listed in Table VII. From our measurement assuming  $\sigma_0 = 1.62 \pm 0.03$  b we get the  $^{42}\text{K}$   $\beta^-$ -decay transition probability  $P_\gamma(1525) = 0.164 \pm 0.004$ . This value disagrees substantially from  $P_\gamma = 0.1808 \pm 0.0009$  measured by Miyahara *et al.* [39] and  $P_\gamma = 0.1813 \pm$

TABLE VII. Previous  $^{41}\text{K}(n,\gamma)$  cross-section measurements.

Author	$\sigma_0$ (b)	$\sigma_\gamma(1525)^a$ (b)
Seren 1947 [42]	$1.0 \pm 0.2$	
Pomerance 1952 [31]	$1.19 \pm 0.10$	
Lyon 1960 [43]	1.45	
Kappe 1966 [44]	$1.50 \pm 0.05$	0.266(8)
Koehler 1967 [45]	$1.2 \pm 0.1$	
Ryves 1970 [46]	$1.46 \pm 0.03$	
Gleason 1975 [47]	$1.43 \pm 0.03$	0.257(5)
Gryntakis 1976 [48]	$1.28 \pm 0.06$	
Heft 1978 [49]	$1.43 \pm 0.03$	0.252(5)
Kaminishi 1982 [41]	$1.57 \pm 0.17$	
De Corte 2003 [50]	$1.42 \pm 0.02$	0.263(2)
Mughabghab 2006 [29]	$1.46 \pm 0.03$	

<sup>a</sup> $\gamma$ -ray cross section from activation experiments.

0.0014 measured by Simoes *et al.* [40] with the  $4\pi\beta\gamma$  coincidence method. These values were used to obtain the recommended value of Mughabghab [29]. Although the cause of this discrepancy is not readily apparent, we note that the  $\sigma_0 = 1.57 \pm 0.17$  b value of Kaminishi and Shuin [41], which agrees with our result albeit with a large uncertainty, was also measured by the  $4\pi\beta - \gamma$  method where corrections for the mass of the source were found to be significant. No such correction was reported by either Miyahara *et al.* or Simoes *et al.*

## V. CONCLUSION

Excellent agreement was found between the relative  $\gamma$ -ray cross sections measured at the Budapest Reactor and the intensity measurements by von Egidy *et al.* [12] and Krusche *et al.* [13,14]. The total measured  $\gamma$ -ray intensity feeding the GS was shown by DICEBOX statistical model calculation to be nearly complete. Although direct neutron capture reactions were thought to be important for these light nuclei, we showed that the primary  $\gamma$ -ray intensities to levels at higher excitation energies could be treated adequately, for most

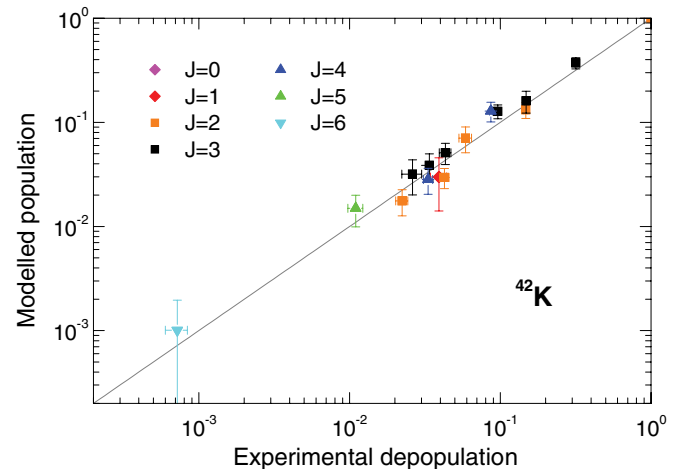


FIG. 5. (Color online) Population-depopulation plot for  $^{42}\text{K}$  obtained assuming the following changes in the spin/parity assignment for low-lying levels:  $J^\pi(783.87) = 3^-$ ,  $J^\pi(841.940) = 3^+$ ,  $J^\pi(1110.747) = 2^-$ ,  $J^\pi(1197.90) = 2^-$ ,  $J^\pi(1254.820) = 3^+$ ,  $J^\pi(1266.305) = 2^+$ ,  $J^\pi(1273.54) = 3^+$ ,  $J^\pi(1377.12) = 1^-$ . Simulations were made with models: SLO for  $E1$ , SP for  $M1$ , and BSGF for level density.

TABLE VIII. Potassium total radiative thermal neutron capture cross sections measured in this work. Two methods were employed to correct the observed feeding to the ground state for the unobserved statistical feeding. An “experimental” value (column Expt.) was determined by correcting the observed ground-state feeding from unplaced and subthreshold  $\gamma$  rays estimated from Monte Carlo simulations. A “statistical” value (column Stat.) was obtained by correcting the ground-state feeding with the calculated statistical feeding from levels above a level excitation energy  $E_{\text{crit}}$  below which the level scheme was presumed to be complete. Both methods give comparable values and the most precise value is adopted here (column Adopted).

Target	$\sigma_{\gamma}^{\text{obs}}$ (b)		$\sigma_0$ (b)		$\sigma_0$ (b)
	GS	Unplaced	Expt.	Stat.	
$^{39}\text{K}$	2.252(16)	<0.056	2.28(4)	2.35(15)	2.28(4)
$^{40}\text{K}$	86(7)	<7	90(8)	90(7)	90(7)
$^{41}\text{K}$	1.604(23)	<0.035	1.62(3)	1.56(15)	1.62(3)

levels, with purely statistical considerations. The simulations of the populations of low-lying levels were in a very good agreement with the experimental populations in most cases and pointed towards discrepancies in the spins and parities of several levels. The observed cross sections corrected for the estimated feedings from unobserved, high-energy transitions are very comparable to those derived from the DICEBOX simulations.

The total radiative neutron cross sections for the potassium isotopes determined in these experiments are summarized in Table VIII where the observed cross sections corrected for the estimated feedings from unobserved, high-energy transitions are very comparable to those derived from the DICEBOX simulations. In Table VIII we give the adopted total radiative neutron cross sections calculated from a weighted average of the statistical and corrected experimental values assuming that 50% of the unplaced transition intensity goes to the GS.

## ACKNOWLEDGMENTS

This work was performed under the auspices of the US Department of Energy by the University of California, supported by the Director, Office of Science, Office of Basic Energy Sciences, of the US Department of Energy at Lawrence Berkeley National Laboratory under Contract No. DE-AC02-05CH11231. Support was also provided by the research plan MSM 002 162 0859 supplied by the Ministry of Education of the Czech Republic by the Czech Science Foundation under Grant No. 13-07117S and by NAP-VEENEUS Contract No. OMFb-00184/2006 of Hungary.

- [1] T. Belgya, Z. Révay, I. H. B. Fazekas, L. Dabolcsi, G. Molnár, J. O. Z. Kis, and G. Kaszás, in *Proceedings of the 9th International Symposium on Capture Gamma-Ray Spectroscopy and Related Topics, Budapest, Hungary, Oct. 8–12*, edited by G. Molnár, T. Belgya, and Z. A. Révay (Springer-Verlag Budapest, 1997), p. 826.
- [2] Z. Révay, T. Belgya, Z. Kasztovszky, J. Weil, and G. Molnár, *Nucl. Instrum. Meth. B* **213**, 385 (2004).
- [3] R. Firestone, H. Choi, R. Lindstrom, G. Molnár, S. Mughabghab, R. Paviotti-Corcuera, Z. Révay, V. Zerkin, and C. Zhou, *Database of Prompt Gamma Rays from Slow Neutron Capture for Elemental Analysis* (IAEA, Vienna, 2007).
- [4] *Handbook of Prompt Gamma Activations Analysis with Neutron Beams*, edited by G. Molnár (Kluwer, Boston, 2004).
- [5] M. Krtička, R. B. Firestone, D. P. McNabb, B. Sleaford, U. Agvaanluvsan, T. Belgya, and Z. S. Révay, *Phys. Rev. C* **77**, 054615 (2008).
- [6] F. Bečvář, *Nucl. Instr. Meth. A* **417**, 434 (1998).
- [7] G. Molnár, Z. Révay, and T. Belgya, *Nucl. Instrum. Meth. Phys. Res. A* **489**, 140 (2002).
- [8] B. Fazekas, J. Óstór, Z. Kis, G. Molnár, and A. Simonits, in *Proceedings of the 9th International Symposium on Capture Gamma-Ray Spectroscopy and Related Topics, Budapest, Hungary, Oct. 8–12*, edited by G. Molnár, T. Belgya, and Z. S. Révay (Springer-Verlag, Budapest, 1997), p. 774.
- [9] Z. Révay and G. Molnár, *Radiochimica Acta* **91**, 361 (2003).
- [10] G. Molnár, Z. Révay, and T. Belgya, *Nucl. Instrum. Meth. Phys. Res. B* **213**, 32 (2004).
- [11] J. Cameron and B. Singh, *Nucl. Data Sheets* **102**, 293 (2004).
- [12] T. von Egidy, H. Daniel, P. Hungerford, H. Schmidt, K. Lieb, B. Krusche, S. Kerr, G. Barreau, H. Borner, R. Brissot *et al.*, *J. Phys. G: Nucl. Phys.* **10**, 221 (1984).
- [13] B. Krusche, K. Lieb, L. Ziegler, H. Daniel, T. von Egidy, R. Rascher, G. Barreau, H. Borner, and D. Warner, *Nucl. Phys. A* **417**, 231 (1984).
- [14] B. Krusche, C. Winter, K. Lieb, P. Hungerford, H. Schmidt, T. von Egidy, H. Scheerer, S. Kerr, and H. Borner, *Nucl. Phys. A* **439**, 219 (1985).
- [15] K. Rosman and P. Taylor, *Pure Appl. Chem.* **70**, 217 (1998).
- [16] N. Bohr, *Nature (London)* **137**, 344 (1936).
- [17] C. Porter and R. Thomas, *Phys. Rev.* **104**, 483 (1956).
- [18] P. Axel, *Phys. Rev.* **126**, 671 (1962).
- [19] D. Brink, Ph.D. Thesis, Oxford University, 1955.
- [20] S. Kadenskij, V. Markushev, and V. Furman, *Sov. J. Nucl. Phys.* **37**, 165 (1983).
- [21] R. Evans, *The Atomic Nucleus* (McGraw-Hill, New York, 1955).
- [22] S. Moszkowski, *Alpha-, Beta-, and Gamma-Ray Spectroscopy*, edited by K. Siegbahn (North Holland, Amsterdam, 1965).
- [23] A. Veysiére, H. Beil, R. Bergère, P. Carlos, A. Leprêtre, and A. D. Miniac, *Nucl. Phys. A* **227**, 513 (1974).
- [24] S. Dietrich and B. Berman, *At. Data Nucl. Data Tables* **38**, 199 (1988).
- [25] R. Capote, M. Herman, P. Obložinský, P. Young, S. Goriely, T. Belgya, A. Ignatyuk, A. Koning, S. Hilaire, V. Plujko *et al.*, *Nucl. Data Sheets* **110**, 3107 (2009).
- [26] T. Belgya, O. Bersillon, R. Capote, T. Fukahori, G. Zhigang, S. Goriely, M. Herman, A. Ignatyuk, S. Kailas, A. Koning *et al.*, Handbook for Calculation of Nuclear Reaction Data, Reference Input Parameter Library-2, Technical Report No. IAEA-TECDOC 1506 (International Atomic Energy Agency, Vienna, Austria, 2006).
- [27] T. von Egidy and D. Bucurescu, *Phys. Rev. C* **72**, 044311 (2005).
- [28] A. Lane and J. Lynn, *Nucl. Phys.* **17**, 563 (1960).
- [29] S. Mughabghab, *Atlas of Neutron Resonances*, 5th ed. (Elsevier, New York, 2006).
- [30] J. Hansen and J. Willard, *Phys. Rev.* **76**, 577 (1949).
- [31] H. Pomerance, *Phys. Rev.* **88**, 412 (1952).
- [32] J. Gillette, ORNL-4013 Report, 1966.
- [33] D. Beckstrand and E. Shera, *Phys. Rev. C* **3**, 208 (1971).

- [34] J. Cameron and B. Singh, *Nucl. Data Sheets* **94**, 429 (2001).
- [35] C. Lister, A. Al-Naser, A. Behbehani, L. Green, P. Nolan, and J. Sharpey-Schafer, *J. Phys. G: Nucl. Phys.* **4**, 907 (1978).
- [36] R. Santo, R. Stock, R. Chapman, and S. Hinds, *Nucl. Phys. A* **118**, 409 (1968).
- [37] B. Singh and J. Cameron, *Nucl. Data Sheets* **92**, 1 (2001).
- [38] M. Unterweger and R. M. Lindstrom, *Appl. Radiat. Isot.* **60**, 325 (2004).
- [39] H. Miyahara, S. Kitaori, Y. Nozue, and T. Watanabe, *Nucl. Instrum. Methods Phys. Res. A* **286**, 519 (1990).
- [40] D. Simoes, M. Kosklinas, and M. Dias, *Appl. Rad. Isot.* **54**, 443 (2001).
- [41] K. Kaminishi and T. Shuin, *Jap. J. Appl. Phys.* **21**, 636 (1982).
- [42] L. Seren, H. Friedlander, and S. Turkel, *Phys. Rev.* **72**, 888 (1947).
- [43] W. Lyon, *Nucl. Sci. Eng.* **8**, 378 (1960).
- [44] D. Kappe, *Diss. Abstr. B* **27**, 919 (1966).
- [45] W. Koehler and H. Schmelz, *Nukleonik* **9**, 270 (1967).
- [46] T. Ryves, *J. Nucl. Energy* **24**, 35 (1970).
- [47] G. Gleason, *Radiochem. Radioanal. Lett.* **23**, 317 (1975).
- [48] J. Kim and E. Gryntakis, *Radiochim. Acta* **16**, 191 (1972).
- [49] R. Heft, in *Proceedings of Computers in Activation Analysis and Gamma-ray Spectroscopy, Mayaguez, Puerto Rico*, 30 Apr–4 May (1978), p. 495.
- [50] F. D. Corte and A. Simonits, *At. Data Nucl. Data Tables* **85**, 47 (2003).